UCRL-17909

cy. 2

University of California

Ernest O. Lawrence Radiation Laboratory

RADIO FREQUENCY STARK SPECTRA OF RbF, RbCl, CsF, CsCl AND NaI

Francis John Lovas
(Ph.D. Thesis)

November 1967

RECEIVED
LAWRENCE
RADIATION
LIBRARY
DOCUMENTS

TWO-WEEK LOAN COPY

This is a Library Circulating Copy which may be borrowed for two weeks. For a personal retention copy, call Tech. Info. Division, Ext. 5545

UCRL-17909
Cy. 2

DISCLAIMER

This document was prepared as an account of work sponsored by the United States Government. While this document is believed to contain correct information, neither the United States Government nor any agency thereof, nor the Regents of the University of California, nor any of their employees, makes any warranty, express or implied, or assumes any legal responsibility for the accuracy, completeness, or usefulness of any information, apparatus, product, or process disclosed, or represents that its use would not infringe privately owned rights. Reference herein to any specific commercial product, process, or service by its trade name, trademark, manufacturer, or otherwise, does not necessarily constitute or imply its endorsement, recommendation, or favoring by the United States Government or any agency thereof, or the Regents of the University of California. The views and opinions of authors expressed herein do not necessarily state or reflect those of the United States Government or any agency thereof or the Regents of the University of California.

UCRL-17909

UNIVERSITY OF CALIFORNIA

Lawrence Radiation Laboratory
Berkeley, California

AEC Contract No. W-7405-eng-48

RADIO FREQUENCY STARK SPECTRA OF RbF, RbCl, CsF, CsCl AND NaI

Francis John Lovas
(Ph.D. Thesis)

November 1967

Acknowledgments 62
Appendicies 63
A. Molecular Beam Detection Studies 63
1. Introduction 63
2. Surface Ionization on Tungsten 65
3. Microwave Discharge Ionization 74
B. Data Retrival System Components 82
C. Dipole Moment Summary Table 83
References 84

RADIO FREQUENCY STARK SPECTRA OF RbF, RbCl, CsF, CsCl AND NaI

Francis John Lovas

Lawrence Radiation Laboratory
University of California
Berkeley, California

November 1967

ABSTRACT

The molecular beam electric resonance method was used to measure the radio frequency Stark spectra of ^{85}RbF, ^{87}RbF, $^{85}Rb^{35}Cl$, CsF, $Cs^{35}Cl$, and NaI. Weak field measurements were made on RbF to obtain accurate hyperfine structure constants. Intermediate to strong field measurements were made on all the above molecules to obtain dipole moment values for the three lowest vibrational states of the J = 1 or 2 rotational state.

Work on a polarizable ion model of the alkali halides which computes dipole moments, the molecular dissociation energy and the second coefficient of the Dunham expansion of the potential energy is also presented. Good agreement with experimental values is obtained.

I. INTRODUCTION

Twenty years after H. K. Hughes constructed the first molecular beam electric resonance (MBER) spectrometer at Columbia University and measured radio frequency Stark transitions in CsF[1] following the suggestion of I. I. Rabi, we see that the state of the art has advanced to the extent that present measurements are about three orders of magnitude more accurate. This is attributed to refined radio-frequency and microwave components and circuits, improved vacuum techniques and many more subtle refinements. J. W. Trischka[2,3,4] improved upon Hughes' spectrometer by introducing a new homogeneous C-field to obtain higher resolution spectra. Subsequent to these original experiments several dozen physicists have contributed significantly to both the theoretical and technical aspects of MBER evolution, as can be seen in the monograph on beam spectroscopy by P. Kusch and V. W. Hughes,[5] and in recent journal articles (many of which will be referred to throughout this thesis). Looking about at present we find at least six independent groups[6-11] investigating the nuclear-electronic interactions in polar diatomic molecules by means of MBER high resolution spectrometers.

While many improvements in MBER techniques have been made, we find one aspect, which has shown little signigicant progress since the first experiments, to be the detection of molecular beams. Surface ionization has been and is the primary method of beam ionization for detection, albeit quite limited in scope with respect to the number of molecules (primarily alkali halides) for which it is sufficiently efficient for MBER studies. The electron bombardment detector or 'universal detector' has yet not been developed sufficiently to be very useful as a MBER detector. The only study reported at present is Weise's work[12] on HF. We have made several endeavors in the direction of improving beam detection in order to extend the MBER method to a wider range of molecules. These will be discussed in Appendix A. Along this same line some improvements in the data retrival system were employed in obtaining the intermediate and strong field Stark spectra of several alkali halides and will be described in Sec. II-E.

However, our primary endeavor has been to continue the measurement of electric dipole moments of alkali halides to high accuracy with a high resolution MBER spectrometer. Presented here will be the radio frequency studies of ^{85}RbF, ^{87}RbF, $^{85}Rb^{35}Cl$, ^{133}CsF, $^{133}Cs^{35}Cl$ and NaI which have yielded accurate dipole moments for low rotational and vibrational states of these molecules, plus other molecular constants such as the quadrupole coupling constants. Work on a polarizable ion model of the alkali halide molecules which predicts dipole moments and their vibrational variation will also be presented.

II. EXPERIMENTAL EQUIPMENT AND TECHNIQUE

A. Introduction

The advantage the MBER method enjoys, similar to other high resolution molecular spectroscopic techniques, lies in its ability to select a single rotational energy state of the species under investigation. When the state is selected one can then observe the hyperfine splittings for a single vibrational energy which are caused by the nuclear-electronic interactions and found in the radio frequency region of the energy spectrum.

The schematic drawing of a typical MBER spectrometer (Fig. 1) shows the beam effusing from the source oven into the main chamber which houses the A and B inhomogeneous electric deflecting (or state selecting) fields, the homogeneous electric C field, the beam collimator and stop, and the beam detector. Depending on the type of state selectors used, the beam is initially focused (A and B quadrupole fields) on the detector, or defocused by the A (dipole) field and then focused on the detector by the B (dipole) field after the molecule has undergone a transition to a new angular momentum orientation in the C field.

A dipole field selects the $(J, \pm m_J)$ state where J is the total angular momentum vector or rotational quantum number and m_J is the projection of J on the field direction or magnetic quantum number. The beam path shown in Fig. 1 is the slection of a molecule in a state with positive effective moment (see Fig. 2) in the A field and focusing it on the detector in the B field after a radio-frequency induced transition in the C field region, if it is now in a state with a negative effective moment. This type of experiment is called "flop-in" because the molecule must flip to a new J orientation before it will be deflected into the detector. Thus an increase in intentisy at the detector is observed when on resonance. This experiment is possible because an inhomogeneous electric field exerts a force on a molecule having a permanent electric dipole moment, μ. This force can be written:

$$F = -\frac{\partial W}{\partial x} = -\frac{\partial W}{\partial E}\frac{\partial E}{\partial x} = \mu_{eff}\frac{\partial E}{\partial x}$$

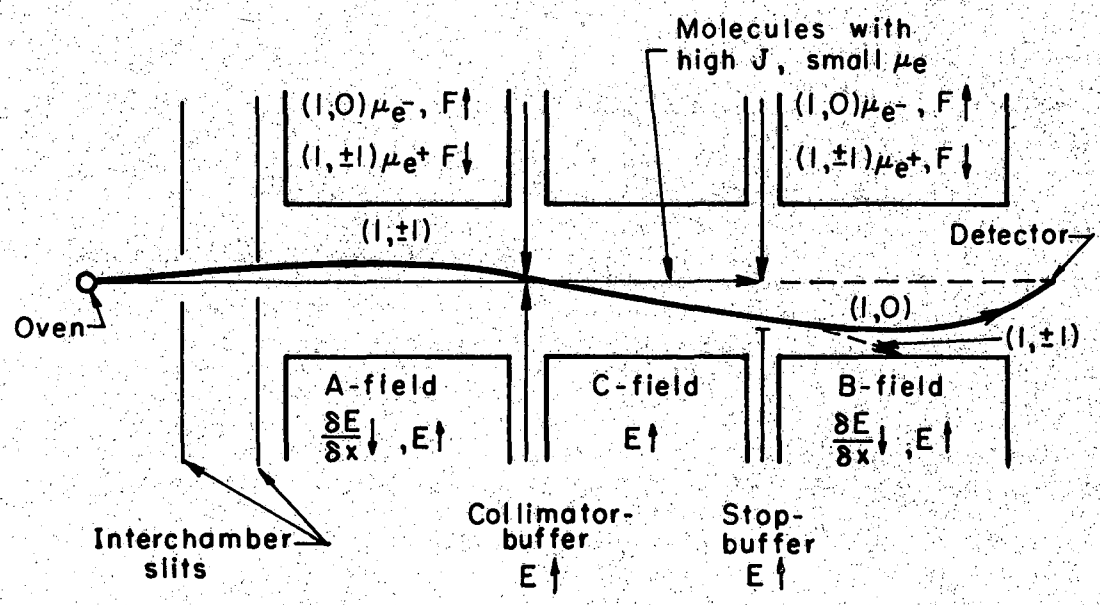

MU-28374-D

Fig. 1. A typical molecular beam electric resonance spectrometer showing the beam path for a "flop-in" experiment at resonance.

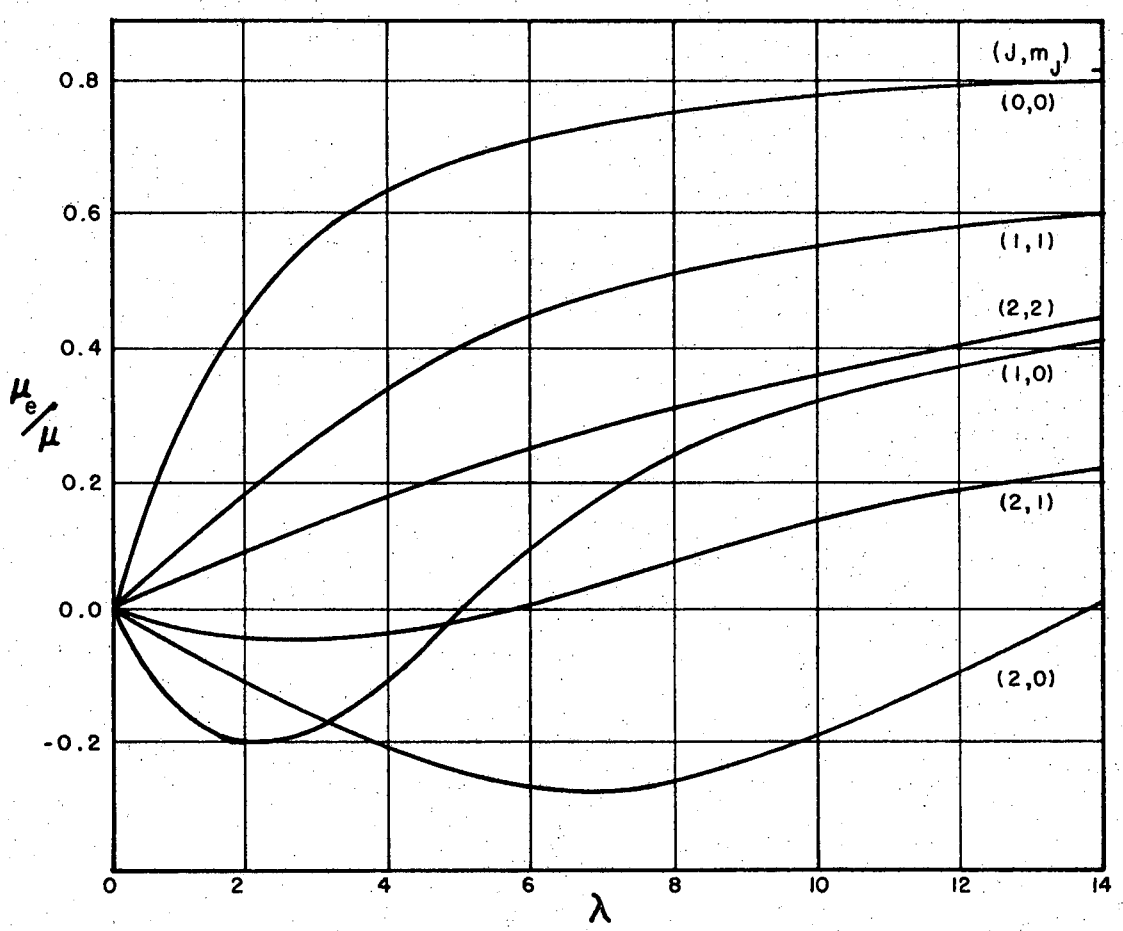

XBL 6711-6033

Fig. 2. The effective electric dipole moment, μ_e, for a rotating polar linear molecule with a permanent dipole moment, μ, in an electric field, E. The dimensionless parameter λ equals $\mu E/B$ where B is the rotational constant. See Ref. 27 for states of higher J quantum numbers.

where W is the energy of the molecule, E the electric field and x is the direction of the field gradient.

The Stark effect is the splitting of the rotational energy level into its $|m_J|$ components caused by the external electric field. In the absence of hyperfine interactions one would observe a single Stark transition in this type of experiment corresponding to the frequency introduced at the C field. The addition of hyperfine structure, i.e. the electronic-nuclear and nuclear-nuclear interactions, causes splitting of the m_J levels and gives rise to multiple resonances. The criteria for observing a resonance is $\Delta|m_J| = |m_J|_A - |m_J|_B \neq 0$ accompanied by a corresponding change in sign of the effective dipole moment.

B. The Spectrometer

These experiments were performed on the spectrometer designed and constructed by A. J. Hebert.[13] Since Hebert has described the apparatus in detail, only significiant modifications and a brief general description will be included here. The vacuum chamber, shown schematically in Fig. 3, consists of four differentally pumped regions referred to as the oven, buffer, main, and electron multiplier chambers. The main chamber holds the two 30.5 cm dipole-analogue inhomogeneous electric deflecting fields, a beam collimator-buffer field, the beam stop-buffer field and the two 25.4 cm homogeneous Stark field parallel plate electrodes. The homogeneous field was made by vapor deposition of 220(18) Å of Aluminum on the two pyrex optical flats which are flat to better than 1/8 wavelength of He light. The flats are held 1 cm apart by three 1.000001(1) cm (at 20°C) gage blocks and have been observed to be parallel to ± 1/8 wavelength of He light along the beam path. One of the electrodes has a razor scratch in the Al deposit at beam position to separate the film for introduction of the radio frequency. In order to eliminate any magnetic couplings due to the earth's magnetic field and the mass spectrometer magnet, we reduced the magnetic field along the beam path in the C field region to less than ± 0.050 G.

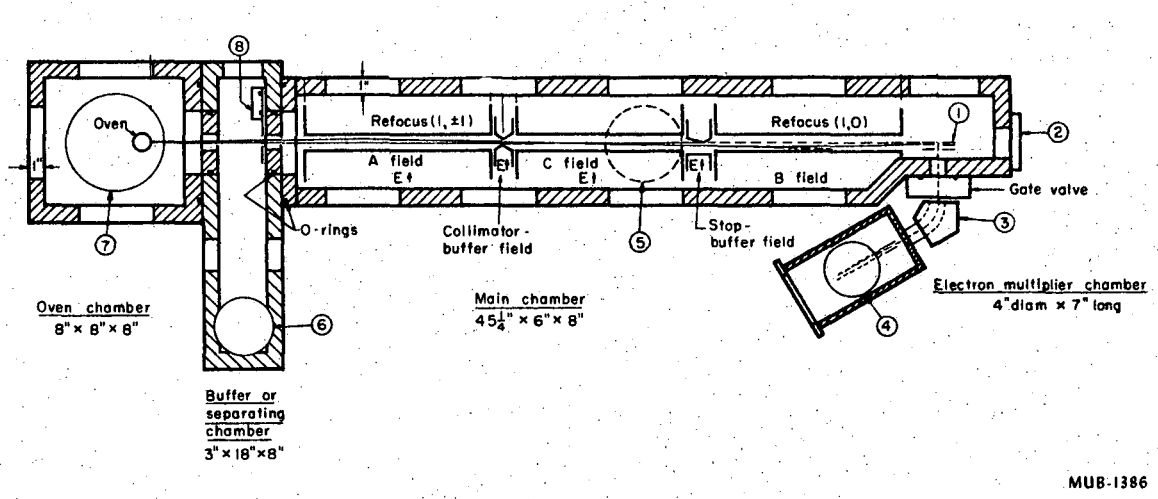

Fig. 3. Schematic diagram (top view) of the electric resonance apparatus. Field lengths and chambers are to scale. Field gaps and beam displacements are exaggerated. Unshaded areas in chamber walls represent access ports.

(1) Surface ionization wire and ion accelerator
(2) Glass port cover for optical alignment
(3) Permanent magnet, 60°, 1-cm gap
(4), (5), (6), (7) Outlets to liquid nitrogen traps and oil diffision pumps
(8) Gate valve and beam flag.

Two oven sources were used in these experiments. One was a 80% platinum and 20% iridium tube (3/8 in. diam by 0.010 in. wall) with a 0.25 in. high by 0.005 in. wide slit. The other oven was a stainless steel tube which had 12 channels separated by 0.075 mm (Fig. 4). This served to conserve source material in addition to giving steady beam intensities for several weeks. Of the molecules studied RbF was the only molecule which reacted with the stainless oven to such an extent that it could not be used.

For detection purposes the beam is dissocated and ionized on the surface of a hot tungsten ribbon and the positive ions are mass-analyzed and focused on a 14-stage electron multiplier for pulse counting or current measurement.

C. Electric Field Measurements

The electric field in the C-region is produced by a 1-6000 V power supply which has given stabilities of 1 ppm/hr. The voltage is measured with a Leeds and Northrup Guarded Potentiometer via a Guidline Volt Ratio Box whose range is 1.5 to 1500 V in 20 steps. The National Bureau of Standards has certified the potentiometer to 1 part in 10^6 and the Volt Ratio Box to 1 part in 10^5. The bank of unsaturated standard cells used for calibration of the potentiometer is certified to 2 parts in 10^6 and is regularly compared with a bank of six saturated standard cells maintained in a thermoregulated air bath by the Electrical Measurement Standards group here. Measurements at NBS have shown the six cells have changed only 1 part in 10^7 in potential over the past six years. The spacing of the C field electrodes is corrected for thermal expansion by thermocouple temperature monitoring of the three gage block spacers and using 8.55×10^{-6} cm/°C.cm as the coefficient of thermal expansion. Table I shows the C field gap variation with temperature for the temperature range in which the experiments were conducted. The temperature varied throughout a day from 22.8°C to 25.0°C. Since the NBS volt differs from the absolute volt, i.e. 1NBS volt = 1.000011(8) absolute volt, the measured voltage must be corrected accordingly if one wishes to be thorough. These uncertainties coupled with the observed inhomogeneities in the C field of ± 7 ppm given an electric field uncertainty of 2 parts in 10^5.

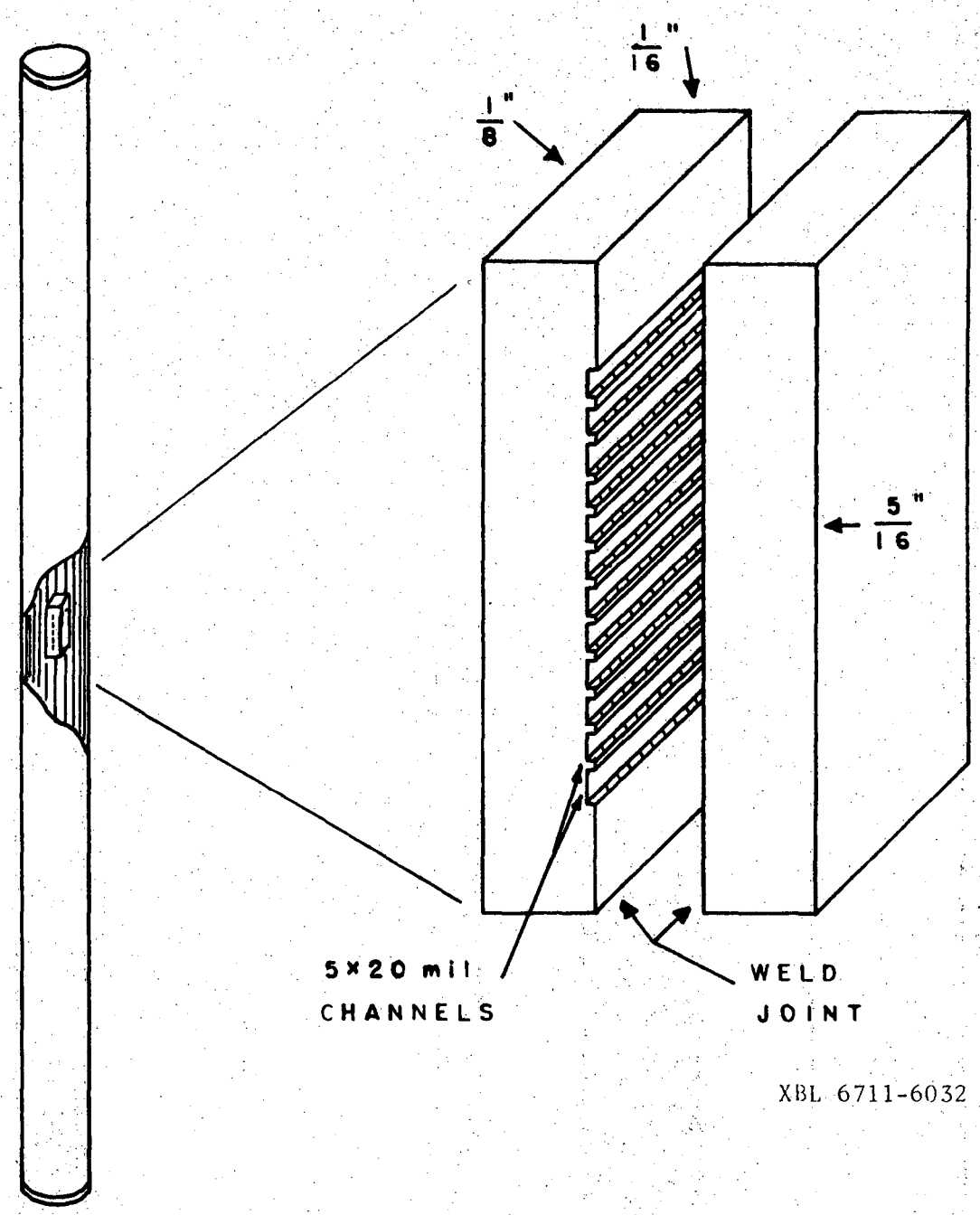

Fig. 4. Molecular beam resistance heated oven with a channel aperture.

Table I. Stark field gap variation with temperature due to gage block expansion. The Al film thickness is taken into account.

Spacer Temperature	Gap
20.0°C	0.9999967(12) cm
21.0°C	1.0000053(13) cm
22.0°C	1.0000138(14) cm
23.0°C	1.0000224(15) cm
24.0°C	1.0000309(16) cm
25.0°C	1.0000395(17) cm

D. Radio Frequency System Used for RbF Experiments

The Hewlett-Packard 606A and 608C radio frequency generators are used to produce signals from 50 kHz to 65 MHz and from 10 MHz to 480 MHz, respectively. These signals are monitered with a H-P 5245L-5253B electronic counter. Pulses from the electron multiplier are amplified and fed into a H-P 5245L-5253A counter. The radio frequency count is printed in the first seven channels of a H-P 562A digital recorder and the beam intensity is printed in the remaining four channels of the recorder. The analog output of the digital recorder for three of the four beam intensity channels is used to drive a Leeds and Northrup pen recorder for graphic representation of the spectrum. A fixed radio frequency is introduced into the transition region while the beam intensity is counted for 1 sec. The counter signals are then printed simultaneously while the frequency is automaticly increased via the print and the counting cycle is restarted.

E. Multichannel Analyzer Data Retrival System

The measuring system just described is extremely sensitive to source pressure and ambient vacuum pressure fluctuations. For this reason it is desirable to employ a system which would reproducibly and rapidly scan the frequency region of interest in order to reduce the effect of these fluctuations. In addition, repetition of this scan for a period of a half hour or more should cause significant improvement in the signal to noise ratio compared to the previous system since a statistical reduction in noise occurs because statistical noise is proportional to the square root of the counts for one standard deviation whereas the resonance signal is proportional to the counts. A block diagram of such a system, which was used for all the molecules studied except RbF, is shown in Fig. 5. The basic idea is to produce a linear frequency sweep which corresponds to a programed sweep of a multichannel analyzer into which the pulses from the electron multiplier are fed.

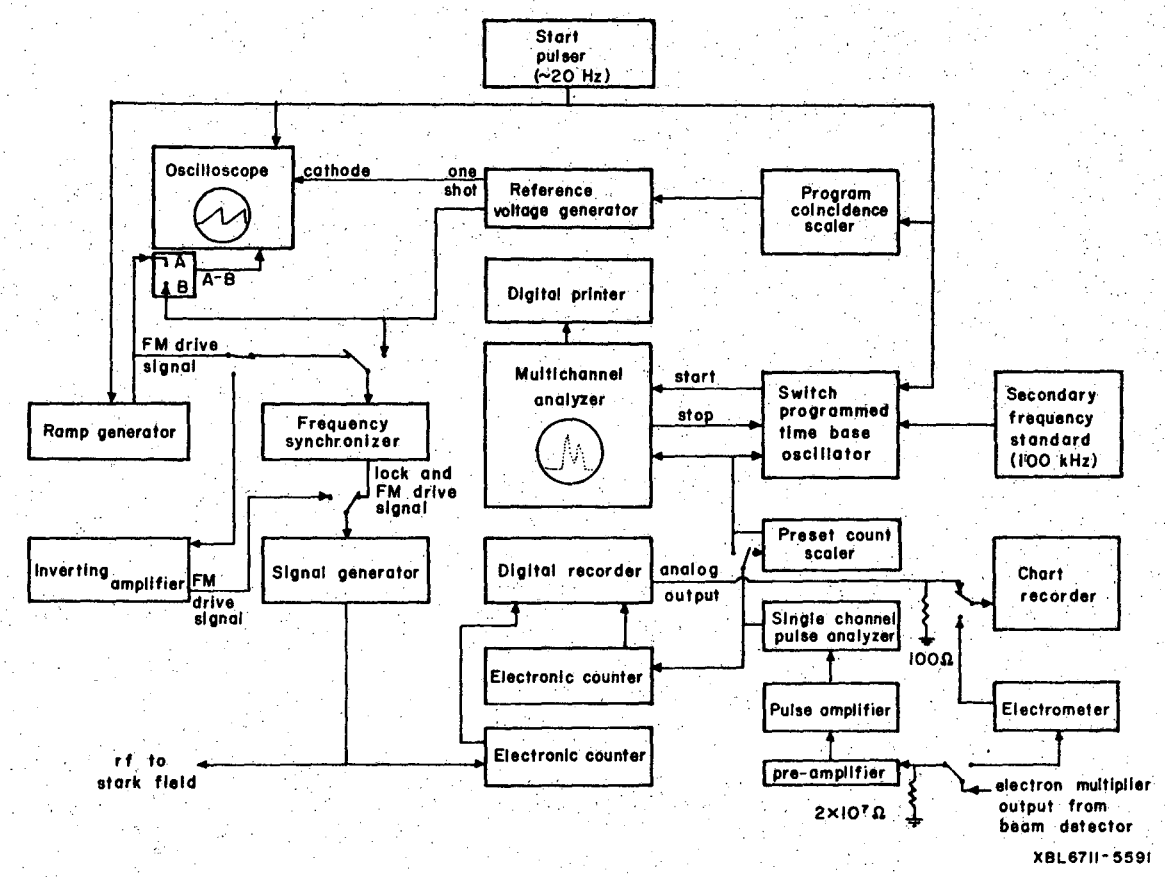

Fig. 5. Block diagram of the electronics for the multichannel analyzer data acquisition system. (Components are listed in Table B-I).

1. Frequency Modulation and Data Storage

A start pulse serves as trigger for the oscilloscope, time base oscillator, and ramp voltage generator. The radio frequency sweep is set at the beginning of a run by means of the variable D.C. ramp potential which serves to frequency modulate the signal generator (H-P 606B or 608F) via the H-P 8708A synchronizer which locks the frequency of the generator at discrete frequencies.

It is possible to bipass the synchronizer and modulate the signal generator directly by using an inverting amplifier to invert the ramp potential for input to the generator. Although this is less accurate due to drift of the signal generator, a wider frequency sweep is obtainable (about a factor of five greater than when locked) for line searches or when very broad lines are observed. The maximum frequency modulation is frequency dependent (see Table II) and thus, at low frequencies one can not sweep the entire range between successive lock points. However, by operating one locked signal generator at a constant frequency, e.g. 65 MHz on the 606B, and the other signal generator at $65 + \nu_{desired}$ MHz and then feeding both signals into a H-P 105144A mixer, one can obtain very wide modulation at any frequency desired with only a 7 decibel power loss.

The repetition rate of the ramp can be set as desired by varying the zero to maximum potential time for the ramp and the start pulse rate which triggers each new sweep. The most satisfactory ramp duration was 50 msec with about 6 msec fall off time and the start trigger at about 15 Hz. These conditions require fast response time from the surface ionization detector for good results.

The trigger signal also starts the multichannel analyzer sweep by means of the time base oscillator which programs the analyzer's "live" or count accepting time per channel and "dead" or channel advance and memory storage time. The dead time for the Northern analyzer used is 2×10^{-5} sec per channel, or 5 msec for 256 channels. This is 10% of the total frequency sweep time. Thus, one has a total useful time loss equal to the sum of the dead time, ramp discharge time (5 msec) and delay time until the next trigger pulse occurs (5 msec) which is about 25% of the actual run time.

Table II. Frequency modulation characteristics of HP-606B and HP-608F signal generators operating in various modes.

Basic Frequency (MHz.)	Maximum Frequency Modulation (kHz.)				
	Locked		Unlocked		Mixer
	606B	608F	606B	608F	606B at 65 MHz.
0.1	0.3	--	1.4	--	310
0.3	0.7	--	4.4	--	310
1.5	5.0	--	--	--	320
3.0	9.0	--	32	--	330
7.5	13	--	50	--	355
15.0	75	30	440	160	385
20.0	60	49	78	400	410
40.0	142	120	670	820	510
80.0	--	283	--	1150	810
160.0	--	553	--	3300	--
320.0	--	1110	--	5500	--

2. Frequency Calibration of the Multichannel Analyzer

The frequency measurement is performed by matching the ramp potential corresponding to a single channel with a reference potential which is then fed into the synchronizer to give a frequency reading on the counter. A single channel is dialed on the programed coincidence oscillator which in turn produces a signal that gives a "bright spot" corresponding to the potential of that channel on the oscilloscope display of the ramp signal. By using a type D oscilloscope plug-in which has a null comparison capability in the A-B mode, one can compare the ramp signal applied to imput A with the reference signal applied to imput B. Adjusting the reference signal until the bright spot is at the null point, one reproduces the potential corresponding to a single channel of the analyzer. This is then applied to the synchronizer-signal generator combination to give a frequency measurement.

Thus, this system allows one to continuously sweep a desired frequency region for any length of time desired on order to improve the signal to noise ratio of weak resonances by reducing the observed noise to that expected from the spectrometer electronics. The average run time was about one hour at a signal level of 20 kcounts/sec using 256 channels. The signal to noise enhancement over the method used for the RbF experiments was approximately a factor of five for a one hour run. This was determined by a direct comparison of a run using both systems on several resonances in CsF. The greatest source of error proved to be the frequency measuring system due to stability limitations in the various components. See Appendix B for a more complete description of the equipment used.

III. THEORETICAL ANALYSIS OF MBER SPECTRA

A. The Hamiltonian for Polar Diatomic Molecules

A rotating and vibrating polar diatomic molecule in a $^1\Sigma$ electronic state has the following Hamiltonian operator when the molecule is in an electric field:[5,14]

$$\mathcal{H} = B\underset{\sim}{J}^2 - \underset{\sim}{\mu}\cdot\underset{\sim}{E} - eq_1Q_1 \frac{[3(\underset{\sim}{I}_1\cdot\underset{\sim}{J})^2 + \frac{3}{2}(\underset{\sim}{I}_1\cdot\underset{\sim}{J}) - (\underset{\sim}{I}_1^2\,\underset{\sim}{J}^2)]}{2I_1(2I_1-1)(2J-1)(2J+3)}$$

$$- e\,q_2Q_2 \frac{[3(\underset{\sim}{I}_2\cdot\underset{\sim}{J})^2 + \frac{3}{2}(\underset{\sim}{I}_2\cdot\underset{\sim}{J}) - (\underset{\sim}{I}_2^2\,\underset{\sim}{J}^2)]}{2I_2(2I_2-1)(2J-1)(2J+3)} + C_1(\underset{\sim}{I}_1\cdot\underset{\sim}{J}) + C_2(\underset{\sim}{I}_2\cdot\underset{\sim}{J})$$

$$+ C_3 \frac{[3(\underset{\sim}{I}_1\cdot\underset{\sim}{J})(\underset{\sim}{I}_2\cdot\underset{\sim}{J}) + 3(\underset{\sim}{I}_2\cdot\underset{\sim}{J})(\underset{\sim}{I}_1\cdot\underset{\sim}{J}) - 2(\underset{\sim}{I}_1\cdot\underset{\sim}{I}_2)\,J(J+1)]}{(2J-1)(2J+3)} + C_4(\underset{\sim}{I}_1\cdot\underset{\sim}{I}_2) \quad .$$

the moment of inertia of the molecule. The second term represents the interaction of the permanent dipole moment, μ, with the external electric field. Due to its dependence on the internuclear separation, μ also exhibits vibrational dependence. The third and fourth terms give the interaction of the nuclear quadrupole moments, Q_1 and Q_2, with the gradient of the molecular electric field at each nucleus, q_1 and q_2, where e is the electronic charge and I_1 and I_2 are the nuclear spins of the two nuclei. The spin-rotation interaction for each nucleus is represented by the fifth and sixth terms. These terms can be interpreted as the interaction of the nuclear magnetic moment with the effective magnetic field produced by the molecular rotation. The last two terms represent the tensor and scalar portions, respectively, of the magnetic (spin-spin) interaction of the nuclei with each other.[15,16] There are additional magnetic interaction terms which arise when an external magnetic field is applied; they are discussed by Gräff and Drechsler.[16] However, these terms are negligible for the present experiments since the magnetic field in the transition region is quite small, as mentioned previously.

B. Energy Eigenvalue Calculation

A computer program[17] sets up a matrix of $\mathcal{H}$ in a $(J, I_1, I_2, m_J, m_{I_1}, m_{I_2})$ representation where m_J, m_{I_1}, and m_{I_2} are the projections of the subscripted angular momentum vectors on the direction of the electric field, E. This matrix is then diagonalized to produce the energy eigenvalues, the frequencies of the spectral lines and their relative intensities using the selection rule $\Delta m_F = 0, \pm 1, \pm 2, \ldots$ where m_F is the projection of the total angular momentum, F, on the field direction. Since m_F is a good quantum number at all values of the electric field, there are no matrix elements connecting states with different values of m_F and the matrix is diagonal in m_F; this fact is utilized to reduce computing time.

The original program contained quadrupole matrix elements diagonal in J as well as some connecting J with J+2 for the eq_2Q_2 term only. Since several molecules studied here have sizable eq_1Q_1 values, those matrix elements off diagonal in J were added for nucleus 1 also. The size of the effect was less than the experimental error at intermediate and strong fields, causing shifts of ±5 kHz at 150 MHz for NaI. The effect will be most important at weak fields when both nuclei have quadrupole coupling constants of large magnitude, e.g. RbBr and RbI. Since this change did not cause a noticeable difference in computing time and since it makes the calculation more accurate, this form of the program is used for all computations.

The first term is diagonal in J and the last four terms are small, thus, only elements diagonal in J are included for these terms. The non-zero matrix element of the Stark interaction takes the form $(J, m_J | \mu \cdot E | J \pm 1, m_J)$. The matrix is limited in J as follows: for a J=1 eigenvalue calculation only the first four J states are included; for a J=2 calculation the first five J states are allowed; and so on. This treatment seems to be better than a fourth order perturbation treatment for the Stark operator and second order in the quadrupole operator.

This method has one disadvantage in that the size of the matrix becomes quite large, especially when J=2 calculations are performed for molecules of sizable nuclear spins, as for CsCl and RbCl. A single J=2 CsCl calculation on the CDC 6600 computer (about four times the speed and memory capability of the IBM 7094) takes about 15 min to diagonalize a 92 × 92 matrix. For this reason J=1 spectra are most desirable when obtainable; the J=1 calculation takes only two minutes.

IV. EXPERIMENTAL SPECTRAL DATA AND DISCUSSION FOR SEVERAL ALKALI HALIDE MOLECULES

In the following discussion the Stark field values are referred to in terms of the voltage applied to the C field electrode as measured with the standard cell--volt box--potentiometer network. The field value is then calculated from the known gap dimension (Table I) as described previously. Great care was taken to maintain reliable field measurements. This involved periodic observation of one of the ^{6}LiF doublets at 600 V whose position is known to high accuracy.[18] It is worth noting here that this C field has no measurable contact potential since the leads are of aluminum and are an integral part of the aluminum film, so that no connectors are needed.

Unless otherwise indicated the spectra are for the J=1 rotational state.

A. The Radio Frequency Spectra of ^{85}Rb^{19}F and ^{87}Rb^{19}F

1. Weak Field Results and Discussion

The MBER radio frequency weak field spectra of RbF has been measured by a number of investigators[19,20,11] to obtain the hyperfine structure (hfs) parameters. The microwave spectra has been measured by several workers[22,23] and recently Stark and Zeeman spectra have been reported.[24] The tables in this section compare the present work with the more accurate work of Zorn et al.[11] and Bonczyk[20] and Hughes.[19,20]

The Stark field used in these experiments was 30 V/cm and the full-width at half-maximum (FWHM) of the observed lines was approximately 2 kHz, consistent with the expected uncertainty-principle linewidth. The signal to noise ratio of the v = 0 lines was 7/1 for the best measurements.

From the apparatus imposed selection rule of $\Delta m_J = \pm 1$, observed singlet linewidth, and transition intensity considerations, one expects 21 lines for the ^{85}RbF(v=0), 16 of which were seen, and 12 lines for ^{87}RbF(v=0), 5 of which were seen. In addition, "forbidden" or $\Delta m_J = 0$ transitions were observed, 4 for ^{85}RbF and 3 for ^{87}RbF. These are non-

adiabatic transitions[19,11] which occur in the A-C and B-C interfield regions. These transitions involve levels characterized by the same F_1 and m_F values. More specifically, using the notation (F_1,m_F,m_J), the levels involved are (7/2,2,0) and (7/2,2,±1) for ^{85}RbF and (5/2,1,0) and (5/2,1,±1) for ^{87}RbF. At low field strengths each of these levels is close, within 10 kHz, to an adjacent level of different $|m_J|$ orientation, making it quite easy for non-adiabatic transitions to occur. It was also noticed that two of the ^{85}RbF forbidden transitions required a non-adiabatic transition in the A-C buffer field region and likewise the other two required non-adiabatic transitions in the B-C region in order to be observed, as one might expect statistically. These transitions are actually quite useful in the sense that one has more measured lines with which to determine the molecular properties, although one suffers a corresponding loss in intensity of the allowed lines since states selected by the A-field contribute to the forbidden transitions and thus cause disagreement between the calculated and observed relative line intensities.

The observed and calculated line positions used in the analysis of the spectra are given in Tables III, IV, and V for ^{85}RbF and Table VI for ^{87}RbF. A typical line is shown in Fig. 6. Three or more measurements were made for each line to produce the average values in these tables. The standard deviation of the measurements for each line were considerably less than the error in determining the line center frequency for an individual measurement due to the relatively low signal to noise ratio. The average line error was about 500 Hz so that the fit of calculated to observed line frequencies is reasonably good.

The values of the hfs parameters derived from these spectral lines are given in Table VII for ^{85}RbF and in Table VIII for ^{87}RbF. The agreement of the ^{85}RbF quadrupole coupling constants with those reported by Zorn et al.[11] is excellent. The other hfs coupling constants agree within experimental error with values reported by all the other investigators.[19-20] The agreement of the v = 0 quadrupole coupling constant for ^{87}RbF with the value reported by Bonczyk and Hughes[20] is not as good, although the rest of the hfs parameters agree within experimental error.

Table III. Calculated and observed line positions for the J = 1, v = 0 radio frequency spectra of ^{85}RbF at E_C = 30 V/cm. All positions are given in kHz.

Line No.	Calculated Line Position	Observed Line Position	Differences (Calc.-Obs.)	Relative Intensity (calc.)
1a	21259.76	21259.27	0.49	4
1b	21254.67	21254.80	-0.13	5
1c	21198.23	21198.22	0.01	9
1d	21114.34	21114.56	-0.22	30
1e	21108.50	21108.37	0.13	30
1f	20933.17	--	--	8
1g	20926.68	20926.81	-0.13	8
1h	14609.86	14610.07	-0.21	90
1i	14602.41[a]	14603.88	-1.47	90
1j	6308.32	6308.12	0.20	15
1k	6303.64[a]	6303.41	0.23	40
1l	6284.98	6284.74	0.24	100
1m	6280.05	6279.99	0.06	13
1n	6275.37	6275.20	0.17	7
1o	6258.25	6258.19	0.06	54
1p	6246.77[a]	6246.69	0.08	57
1q	6228.07	6228.22	-0.15	3
1r	6213.58	6213.69	-0.11	8
1s	117.16[a]	117.02	0.14	16
1t	114.05	113.96	0.09	16

[a]These are $\Delta m_J = 0$ forbidden transitions (see text).

Table IV. Calculated and observed line positions for the J = 1, v = 1 radio frequency spectra of ^{85}RbF at E_C = 30 V/cm. All positions are given in kHz.

Line No.	Calculated Line Position	Observed Line Position	Differences (Calc.-Obs.)	Relative Intensity (calc.)
2a	21027.75	--	--	4
2b	21022.73	--	--	5
2c	20964.89	--	--	9
2d	20879.14	20878.92	0.22	30
2e	20873.09	20873.00	0.09	30
2f	20693.85	20693.86	-0.01	8
2g	20687.03	20687.03	0.00	8
2h	14441.24	14441.25	0.01	90
2i	14433.86[a]	14434.18	-0.32	90
2j	6237.30	6237.35	-0.05	15
2k	6232.50[a]	6232.52	-0.02	40
2l	6213.47	6213.69	-0.22	100
2m	6208.49	6208.42	0.07	13
2n	6203.64	--	--	7
2o	6185.95	6185.79	0.16	54
2p	6174.26[a]	6174.32	-0.06	57
2q	6145.37	--	--	3
2r	6141.26	6141.13	0.13	5
2s	119.95[a]	119.87	0.08	16
2t	116.77	117.02	-0.25	16

[a]These are $\Delta m_J = 0$ forbidden transitions (see text).

Table V. Calculated and observed line positions for the J = 1, v = 2 radio frequency spectra of ^{85}RbF at E_C = 30 V/cm. All positions are given in kHz.

Line No.	Calculated Line Position	Observed Line Position	Differences (Calc.-Obs.)	Relative Intensity (calc.)
3a	20797.59	--	--	4
3b	20793.98	--	--	5
3c	20734.68	--	--	9
3d	20646.00	20646.43	-0.43	30
3e	20640.80	20640.37	0.43	30
3f	20456.46	--	--	8
3g	20450.44	--	--	8
3h	14274.41	14274.49	-0.08	90
3i	14267.11[a]	14267.35	-0.24	90
3j	6167.45	--	--	15
3k	6162.20[a]	6162.49	-0.29	40
3l	6141.64	6141.13	0.51	100
3m	6137.60	--	--	13
3n	6131.75	--	--	7
3o	6113.77	6114.20	-0.43	54
3p	6102.98[a]	6103.22	-0.24	57
3q	6072.50	--	--	3
3r	6068.49	6068.58	-0.09	8
3s	122.78[a]	122.71	0.07	16
3t	119.58	119.87	-0.29	16

[a]These are $\Delta m_J = 0$ forbidden transitions (see text).

Table VI. Calculated and observed line positions for ^{87}RbF in the J = 1 state at E_C = 30 V/cm. All positions are given in kHz.

		Calculated	Observed	Differences	Intensity
v = 0:		Observed line error is ± 0.20 kHz.			
	1a	8444.29	8444.22	0.07	100
	1b	8437.08[a]	8437.18	-0.10	99
	1c	6715.93[a]	6715.95	-0.02	85
	1d	6712.03	6712.10	-0.07	10
	1e	6700.92[a]	6701.00	-0.08	96
	1f	6696.23	6696.16	0.07	97
	1g	166.34[a]	165.80	0.54	22
	1h	161.47	161.29	0.18	22
v = 1:		Observed line error is ± 0.30 kHz.			
	2a	8347.85	8347.84	0.01	100
	2b	8340.96[a]	9340.99	-0.03	99
	2c	6636.49[a]	--	--	85
	2d	6633.25	--	--	10
	2e	6623.04[a]	6622.10	-0.06	96
	2f	6618.65	6618.63	0.02	97
	2g	170.17[a]	169.91	0.26	22
	2h	165.60	165.80	-0.20	22
v = 2:		Observed line error is ± 0.7 kHz.			
	3a	8266.44	8265.8	0.64	100
	3b	8259.59[a]	8260.0	-0.41	99
	3c	6571.96[a]	--	--	85
	3d	6568.72	--	--	10
	3e	6558.53[a]	6558.2	0.33	96
	3f	6554.12	6553.6	0.52	97
	3g	174.20[a]	--	--	22
	3h	169.61	169.91	-0.30	22

[a]These are $\Delta m_J = 0$ forbidden transitions (see text).

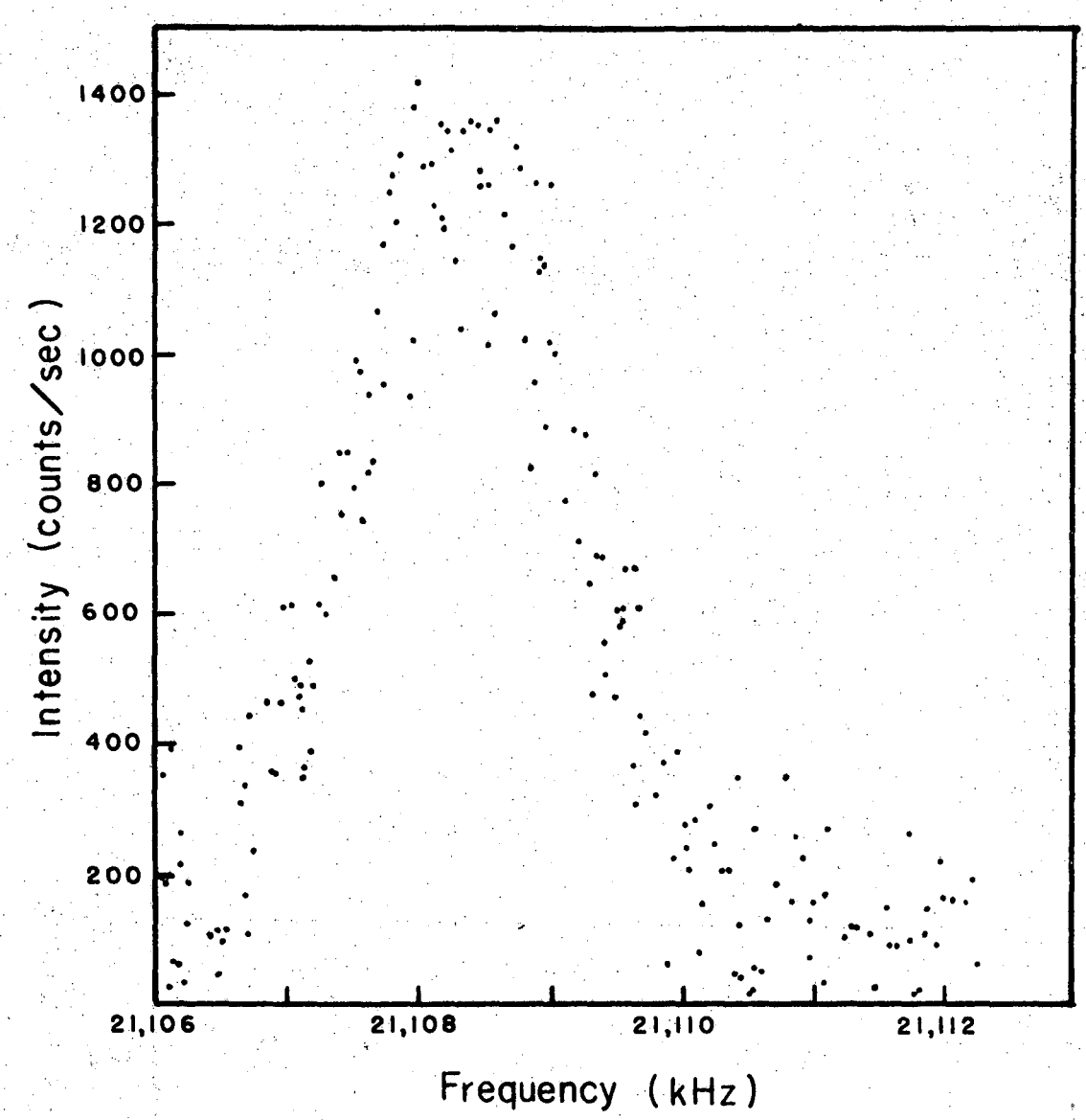

XBL 6711-6039

Fig. 6. A typical ^{85}RbF J = 1, v = 0 line for Stark field of 30 V/cm.

Table VII. Hyperfine coupling constants for the J = 1 state of $^{85}Rb^{19}F$ at E_C = 30 V/cm.

v	eq_1Q_1(MHz)	c_1(kHz)	c_2(kHz)	c_3(kHz)	c_4(kHz)
0	-70.3419(20)	0.45(10)	10.55(50)	0.94(20)	0.20(20)
1	-69.5564(30)	0.47(15)	10.8(10)	0.9(4)	0.3(3)
2	-68.7795(50)	0.5(2)	10.1(14)	1.0(7)	0.5(10)

Quadrupole Coupling Constant Function

$$(eq_1Q_1)_v = (eqQ)_e + (eqQ)_I\ (v+1/2) + (eqQ)_{II}\ (v+1/2)^2$$

Coefficient	Present	Zorn et al.[11]
$(eqQ)_e$	-70.7380(48) MHz	-70.739 MHz
$(eqQ)_I$	0.7943(85) MHz	0.797 MHz
$(eqQ)_{II}$	- 0.0044(40) MHz	- 0.005 MHz

Table VIII. Hyperfine coupling constants for the J = 1 state of $^{87}Rb^{19}F$ at E_C = 30 V/cm.

v	eq_1Q_1(MHz)	c_1(kHz)	c_2(kHz)	c_3(kHz)	c_4(kHz)
Present Work					
0	-34.0343(20)	1.65(20)	10.5(9)	2.9(7)	0.7(7)
1	-33.6838(35)	1.70(25)	9.5(15)	2.9(10)	--
2	-33.336(4)	1.45(30)	9.5(15)	2.9(15)	--
Bonczyk and V. Hughes[20]					
0	-34.0313(10)	1.595(50)	10.51(8)	3.16(18)	0.66(10)
V. Hughes and L. Grabner[19]					
0	-34.00(6)		14(4)		
1	-33.63(6)		14(4)		
2	-33.20(6)		--		

Quadrupole Coupling Constant Function

$$(eq_1Q_1)_v = (eqQ)_e + (eqQ)_I\ (v + 1/2)$$

$(eqQ)_e$	-34.2116(45) MHz	-34.20(11)[a] MHz
$(eqQ)_I$	0.3533(40) MHz	0.40(8)[a] MHz
$(eqQ)_{II}$	0.0014(20) MHz	

[a]Calculated from values reported in Ref. 19.

Unfortunately the measurement errors in the RbF quadrupole coupling constants were too large to allow one to look for a nuclear polarizability by comparing the quadrupole moment ratios $Q_{^{85}Rb}/Q_{^{87}Rb}$ in two different molecular environments such as RbF and RbCl (see Table IX). The quadrupole moment ratios for RbCl have not been determined to as high accuracy as have those of RbF. It appears that at least an order of magnitude improvement in accuracy is required in order to begin looking for the nuclear polarizability. Recently Bonczyk and Hughes[20] have compared the ^{79}Br and ^{81}Br quadrupole moment ratios obtained for atomic bromine and in $^{6}LiBr$. The comparison resulted in a difference in ratio of (22 ± 8) parts in 10^5, which is attributed to nuclear polarization. Even here one would be more confident in the reality of the effect if the experimental measurements of the ratios were carried out to greater accuracy.

2. Strong Field Results and Discussion

The strong field spectra were observed at a Stark field of 600 V/cm for ^{85}RbF in order to determine the dipole moment of the three lowest vibrational states. Table X lists the observed and calculated frequencies and Table XI contains the dipole moments derived from these lines as well as the moments reported in the literature. The FWHM for the observed lines was about 28 kHz with no singlets being observable. As in the weak field spectra the frequencies listed are the average of three or more measurements of each line and the calculated lines are the intensity weighted average of the multiple components making up each observed line. Due to this multiplet composition and the inhomogeneities of the Stark field, the linewidths are quite broad compared to the weak field spectra. As can be seen from Table XI the agreement of the present work with that of Gräff et al. is excellent.

Several lines for each vibrational state of ^{87}RbF were measured at 600 V/cm and 750 V/cm to determine the dipole moments. The values obtained were 0.0001 D lower than the corresponding ^{85}RbF values of μ_v, which is not significant since the error is of the order of ± 0.001 D.

Table IX. Quadrupole moment ratios of ^{85}Rb and ^{87}Rb.

$$\chi \qquad \frac{Q_{85}}{Q_{87}} = \frac{(eq_1Q_1)_{\chi\ 85_{Rb}}}{(eq_1Q_1)_{\chi\ 87_{Rb}}}$$

	RbF[a]	RbF	RbCl
v = 0	2.06679(18)	2.06694(6)[20]	2.0669(5)[21]
v = 1	2.06498(30)		
v = 2	2.06322(50)		
equilibrium	2.06766(45)		

[a]Present work.

Table X. Calculated and observed line positions for ^{85}RbF in the J = 1 state at E_C = 600 V/cm. All positions are given in kHz.

Line	Calculated	Observed	Differences	Intensity
v = 0				
a	173388.78	173387.32	1.46	56
b	169913.38	169912.23	1.15	70
c	169543.09	169531.65[a]	11.44	44
d	166067.69	166065.87	1.82	1
e	159731.14	159730.08	1.06	100
f	157760.36	157758.42	1.94	29
g	155396.81	155397.20	-0.39	44
h	154944.10	--	--	15
i	151551.12	151553.30	-2.18	56
j	151423.80	151421.55	2.25	1
k	146944.5	146943.1	1.4	100
l	142791.1	142788.5	2.6	70
v = 1				
a	176769.73	176770.00	-0.27	56
b	173324.90	173323.92	0.98	70
c	172961.92	--	--	44
d	169517.15	169531.65[a]	-14.50	1
e	163251.06	163248.62	2.44	100
f	161311.01	161311.67	-0.66	29
g	158978.56	158981.33	-2.77	44
h	158531.11	158532.18	-1.07	15
i	155170.43	155171.97	-1.54	56
j	155045.06	155045.45	-0.39	1
k	150626.52	150624.80	1.72	100
l	146517.0	146513.3	3.7	70
v = 2				
a	180234.0	180231.3	2.7	56
b	175820.28	176819.95	0.33	70
c	176463.48	--	--	44
d	173049.71	--	--	1
e	166853.64	166852.42	1.22	100
f	164944.00	--	--	29
g	162641.53	162651.75	-0.22	44
h	162199.32	--	--	15
i	158870.96	158871.88	-0.92	56
j	158747.93	158751.82	-3.89	1
k	154389.05	154388.75	0.30	100
l	150323.04	--	--	70

[a]The two component lines were not resolved.

Table XI. Dipole moments for $^{85}Rb^{19}F$ in the J = 1 state. All values are given in Debye.

	Present[a] (600 V/cm)[b]	Gräff et al.[24]	Lew et al.[22]
μ_0	8.5465(5)	8.5464(17)	8.80(10)
μ_1	8.6134(7)	8.6127(17)	
μ_2	8.6809(9)		
	$\mu_v = \mu_e + \mu_I(v + 1/2) + \mu_{II}(v + 1/2)^2$		
μ_e	8.5131(7)	8.5132[c]	
μ_I	0.06650(28)	0.0663[c]	
μ_{II}	0.00026(12)		

[a]The accuracy of the dipole moments is limited by the uncertainty in the absolute value of the electric Stark field; however, the precision of the results is at least a factor of five better and allows smaller errors to be reported for the coefficients in the dipole moment expression.

[b]Calculations were made with the field in absolute units, assuming that one NBS volt equals 1.000011 absolute volts.

[c]Calculated here for comparison.

B. The Radio Frequency Spectra of $^{133}Cs^{19}F$

These measurements were performed with the computer averaging techique mentioned earlier. The frequency sweep or modulation was 300 kHz at 160 MHz. Since the sweep signal was quite linear, less than 0.1% straight line deviation, only three points were necessary for frequency calibration. Calibration readings were taken before and after each run in order to check possible drift in the oscillator. In order to prevent systematic drifts, each run overlapped the previous one by about 100 kHz. The agreement of overlapping lines in adjacent runs was very good.

The Stark field used here was 600 V/cm and the observed FWHM line width was 27 kHz. A typical v = 0 spectrum is shown in Fig. 7. A modification of the computer calculation of the transition frequencies produces a plot of the experimental spectrum for any chosen line width. By assuming a gausian line shape and adjusting the theoretical line width until the observed line width is obtained, one can produce quite a good fit to the experimental spectrum as evidenced by the calculated v = 0 spectrum in Fig. 8 which required 22 kHz line width. All expected lines were observed for v = 0,1 states and just the stronger lines were seen for the v = 2,3 states.

The hfs coupling constants used to obtain a fit to the spectra were in good agreement, although much less accurate, with those reported by T. English[25] derived from weak field measurements. The dipole moments obtained here are given in Table XII along with values reported in the literature. There is considerable discrepancy between the present more accurate values and those of Gräff et al. This, we suggest, is due to C field measurement errors not reflected in the quoted error of ± 0.003 D. The internal consistency of the present work is evidenced by calculating μ_3 from the dipole moment expression, where the coefficients are obtained from μ_0, μ_1, and μ_2. The value calculated is μ_3 = 8.0972(60). Care was exercised to prevent Stark field measurement error by running ^6LiF spectra as mentioned previously. The error estimates for v = 0 spectra are broken down as follows:

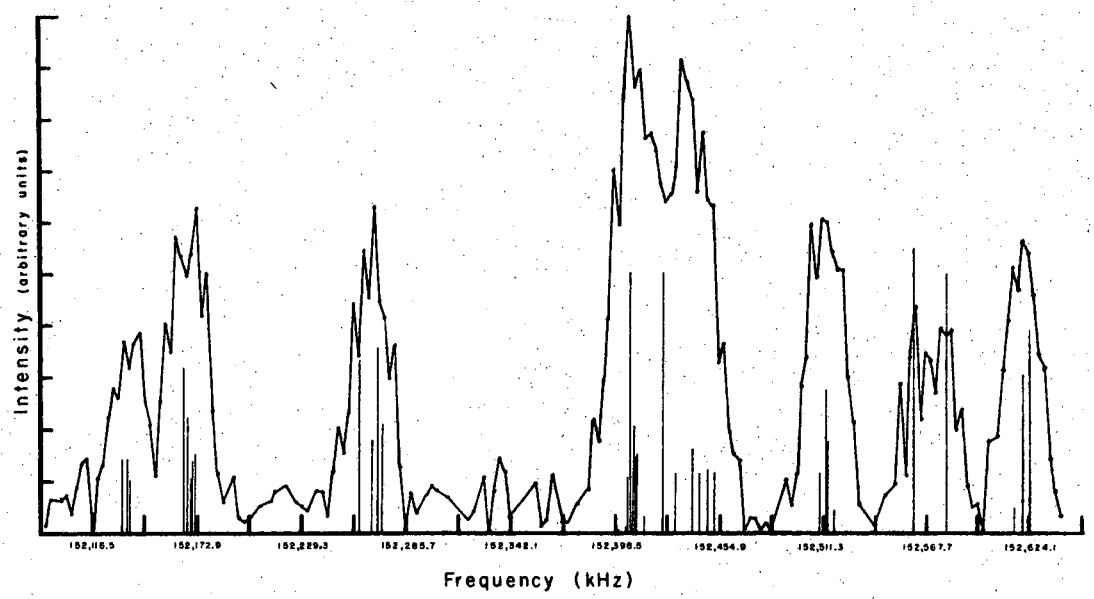

Fig. 7. The observed J = 1, v = 0 spectrum for CsF at a Stark field of 600 V/cm. The vertical lines represent the calculated spectrum.

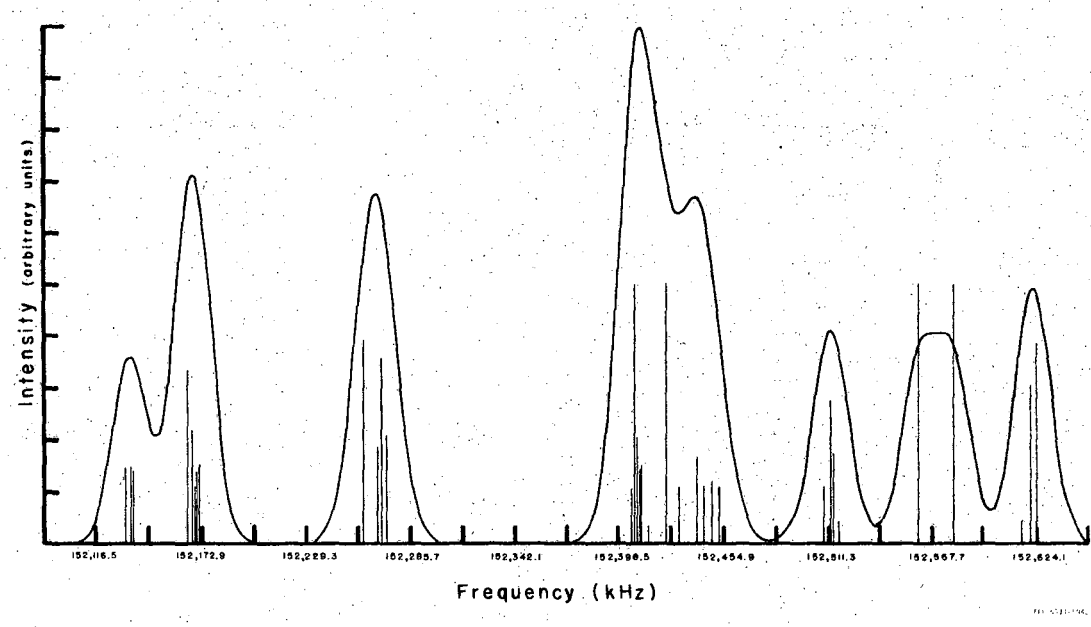

Fig. 8. The calculated J = 1, v = 0 spectrum for CsF at 600 V/cm using a gausian line shape and a line-width at half-maximum of 22 kHz to synthesize the observed spectrum.

Table XII. Dipole moments of $^{133}Cs^{19}F$. All values are given in Debye.

	Present[a] (E_C = 600 V/cm)[b]	Gräff and Runolfsson[26]	Trischka[4]	H. Hughes[1]
μ_0	7.8839(9)	7.876(3)	7.875(6)	7.3(5)
μ_1	7.9546(10)	7.986(3)	7.947(6)[c]	
μ_2	8.0257(12)		8.019(6)[c]	
μ_3	8.0969(15)			
	Dipole Moment Function			
	$\mu_v = \mu_e + \mu_I(v + 1/2) + \mu_{II}(v + 1/2)^2$			
μ_e	7.8486(13)	7.842(3)	7.839(6)[c]	
μ_I	0.07039(30)	0.07229(12)	0.0722(3)	
μ_{II}	0.00018(19)			

[a]The accuracy of the dipole moments is limited by the uncertainties mentioned in the text; however, the precision of the results is at least a factor of five better and allows smaller errors to be reported for the coefficients in the dipole moment function.

[b]Calculations were made with the field in absolute units, assuming that one NBS volt equals 1.000011 absolute volts.

[c]Calculated here for comparison.

25 ppm	C field voltage measurement error
55 ppm	frequency measurement error
23 ppm	line fitting error based on S/N and line width considerations.

C. The Radio Frequency Spectra of $^{85}Rb^{35}Cl$

The hyperfine structure for several vibration states of $^{85}Rb^{35}Cl$ was first measured by Trischka and Braunstein[21] who observed MBER rotational transitions of the $J = 0 \rightarrow 1$ type. That work allowed determination of the nuclear quadrupole coupling constants and spin-rotation constants, but the dipole moments were not measured. The present effort was directed at measurement of the dipole moments of the low vibrational states of the $J = 2$ rotational state. Spectra for the $J = 1$ state which would produce greater accuracy in dipole moment determination could not be observed since molecules in the (1,0) state could not be deflected sufficiently. Transitions of the type $(2,1) \rightarrow (2,0)$ were observed at a static C-field value of 900 V/cm. There was some difficulty in observing these resonances due to the low signal to noise ratio, which proved to be about 2 to 1 for the average two hour run. The line widths were also rather large, about 150 kHz, partially due to the use of the signal generator in the unlocked mode. Even with these difficulties, reasonably accurate dipole moments could be extracted from the data. Table XIII shows the calculated and observed composite line positions along with the calculated relative intensities. The hyperfine values required to produce the calculated spectra were in very good agreement with those reported by Trischka and Braunstein, although the present values were of lower accuracy since weak field spectra were not measured. The dipole moments derived from these spectra are:

$$\mu_0 = 10.510(5) \qquad \mu_1 = 10.564(5) \qquad \mu_2 = 10.618(5)$$

$$\mu_v = 10.483(6) + 0.054(3)(v + 1/2).$$

Table XIII. Calculated and observed line positions for $^{85}Rb^{35}Cl$ for the (2,1) → (2,0) transitions at a Stark field of 900 V/cm.

Line[a]	Calculated	Observed	Calc. Intensity
a_0	110165 kHz		22
a_1	112500		15
b_0	113010	112980 kHz	32
a_2	114600		10
b_1	115175		20
c_0	115420	115365	100
d_0	117400	117370	54
b_2	117420		14
c_1	117570		70
e_0	118090	118085	55
f_0	118490		73
d_1	119530		35
c_2	119780	119782	50
e_1	120220	120130	37
f_1	120625	120568	50
d_2	121740	121676	35
e_2	122400		25
f_2	122810		35
g_0	122890	122957	45
g_1	125000	125048	28
h_0	125300	125336	65
g_2	127120	127213	23
h_1	127390	127450	42
h_2	129490	129519	30

[a]The subscripts refer to the vibrational state.

D. The Radio Frequency Spectra of $^{133}Cs^{35}Cl$

The first radio frequency Stark spectra of CsCl reported by Luce and Trischka[28] in 1953. The accuracy of the dipole moments reported in that paper was limited by the fact that the rotational constant was not well determined. After a more accurate rotational constant was available, the μ_v values were calculable to higher accuracy.[4] Trischka's spectra consisted of one very broad resonance, about 1 MHz FWHM at 115 MHz, for each vibrational state. Thus, only an upper limit estimate of the nuclear quadrupole interaction constants for each nucleus could be made.

The present work was undertaken in order to varify and improve upon the accuracy of this previous work. The spectra observed here consisted of two quite broad lines for each vibrational state of the J = 2 rotational state. The transitions observed were (2,1) → (2,0). Spectra were measured at 150 MHz with a Stark field of 900 V/cm and at 295 MHz for a Stark field of 1200 V/cm. Similar to RbCl, the J = 1 spectra could not be produced due to insufficient deflection of the (1,0) state. Typical spectra are shown in Fig. 9 which are the result of one to two hour runs. Although several clusters of lines were observed here, the resolution at these field values was insufficient for determination of the hyperfine interactions other than a somewhat crude measurement of the quadrupole interactions. The observed line frequencies are shown in Table XIV and the dipole moment values derived from these data are listed in Table XV along with the values found in the literature.

The present dipole moment measurements differ from Trischka's by nearly twice his assumed experimental error. The fact that the μ_I values agree indicates a systematic error in high field measurements. However, this was apparently not the case for the CsF measurements described previously (see Table XII). The present measurement of μ_I for CsF disagrees quite significantly with both measurements previously reported. The same method of fitting the data was identical in both cases here.

The nuclear quadrupole coupling constants used in fitting the calculated and observed spectra were:

$$eqQ_{Cs} = |2.5| \pm 1.0 \text{ MHz} \qquad \text{and} \qquad eqQ_{Cl} = |1.5| \pm 1.0 \text{ MHz},$$

which agree with Trischka's values of $\leq|4|$ and $\leq|3|$ MHz respectively.

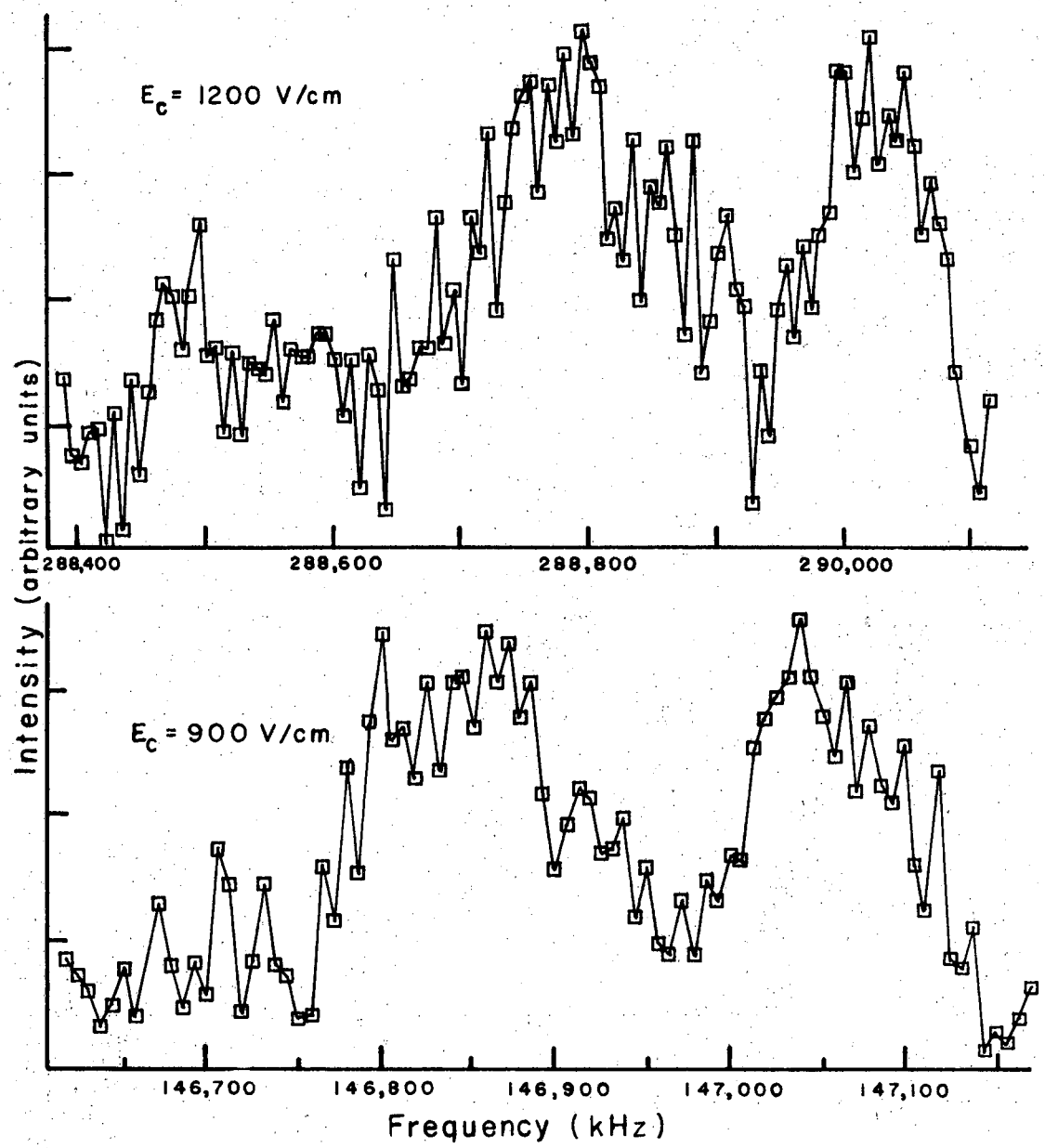

XBL 6711-6038

Fig. 9. The J = 2, v = 0 spectra of CsCl observed at a Stark field of 900 V/cm and 1200 V/cm.

Table XIV. Observed line centers for $^{133}Cs^{35}Cl$ transitions of the type (2,1) → (2,0). All positions are in kHz.

Line		900 V/cm	1200 V/cm
v = 0:			
	a	146,845	288,780
	b	147,060	289,030
v = 1:			
	a	149,610	294,530
	b	149,815	294,760
v = 2:			
	a	152,450	300,370
	b	152,640	300,580

Table XV. Dipole moments of $^{133}Cs^{35}Cl$ for the J = 2 rotational state.

	Present work	Trischka[4]
μ_0	10.387(4)	10.42(2)
μ_1	10.445(4)	10.476(22)[a]
μ_2	10.503(4)	10.532(24)[a]
μ_e	10.358(5)	10.392(25)[a]
μ_I	0.058(1)	0.056(2)

[a]Calculated here from the expression given in Ref. 4.

E. The Radio Frequency Spectra of $^{23}Na^{127}I$

Very little data on the hyperfine interactions in NaI can be found in the literature. Honig et al.[29] have observed the rotational spectrum and obtained quadrupole coupling constants for the lowest four vibrational states for the iodine nucleus and Cote and Kusch[30] have reported the v = 0 quadrupole and spin rotation coupling constants for the sodium nucleus. Recently we have learned of a weak field study by MBER undertaken by C. E. Miller and J. Zorn which was reported at the Ohio State Molecular Spectroscopy Conference in September 1967.

The present experiments were performed at the intermediate field values of 300 V/cm and 450 V/cm in order to determine the dipole moments of the lowest three vibrational states of the J = 1 rotational state. Since the iodine quadrupole coupling constant is very large, the spectrum is spread over a wide frequency range. Due to the fact that rather wide resonance lines were observed, it proved quite satisfactory to measure only four lines for the v = 1 and 2 spectra without loss of accuracy. Measurement of more lines would not permit a more accurate hyperfine structure determination, while the four lines chosen allowed determination of eqQ for both nuclei. The agreement of the calculated and observed lines indicated that the spin-rotation and spin-spin terms were too small to require inclusion in the calculation. This is borne out by the values Miller and Zorn obtained, which were all less than 1 kHz. The nine lines observable between 100 MHz and 146 MHz were measured in the present work for the v = 0 spectra only in order to be certain of the correct assignment of the lines.

The calculated and observed line positions for all three vibrational states observed are listed in Table XVI. The molecular constants derived from this data are shown in Table XVII along with the values from the literature for comparison. This is the first reported measurement of the electric dipole moment for NaI so no comparison is possible.

A summary of the dipole moments reported in this thesis along with all the values reported in the literature can be found in Appendix C.

Table XVI. Calculated and observed line positions for $^{23}Na^{127}I$ in the J = 1 state and E_C = 300 and 450 V/cm. All positions are given in kHz.

Line No.	Calculated	Observed	Calculated	Observed
	300 V/cm		450 V/cm	
v = 0				
a	146278	146285	243941	243961
b	145112	145117	242767	242782
c	137476	137517		
d	136432	136475		
e	136355	136395		
f	135332	135392		
g	127638	127602		
h	126575	126575		
i	107017	107004	197590	197593
j	106041	106022	196457	196489
v = 1				
a	148425	148422	247630	247650
b	147270	147258	246470	246482
i	108610	108607	200665	200665
j	107643	107628	199547	199540
v = 2				
a	150556	150558	251312	251353
b	149424	149412	250175	250192
i	110197	110188	203748	203707
j	109247	109234	202650	202638

Table XVII. Quadrupole coupling constants and dipole moments for $^{23}Na^{127}I$ in the J = 1, v = 0,1,2 states.

	v = 0	v = 1	v = 2	Reference
$eq_1Q_1(Na)$	-4.10(5)	-4.05(5)	-3.98(5)	Present
	-4.072(5)			34
	-3.96			30
$eq_2Q_2(I)$	-262.00(50)	-265.43(50)	-268.80(50)	Present
	-259.87(60)	-264.52(65)	-267.59(40)	29
	-262.140(5)			34
μ_v	9.2357(30)	9.2865(30)	9.3370(30)	Present

$$eq_1Q_1(Na)_v = -4.13 + 0.06(v + 1/2) \pm 0.07 \text{ MHz.}$$

$$eq_2Q_2(I)_v = -260.30 - 3.4(v + 1/2) \pm 0.7 \text{ MHz.}$$

$$\mu_v = 9.2103 + 0.0507(v + 1/2) \pm 0.005 \text{ D.}$$

F. Estimation of Relative Resonance Detection Efficiency

At this point it may be of value to point out the increasing difficulty encountered when attempting to observe spectra of the heavier alkali halides. The gross beam intensity for the heavier molecules is significantly less than that of the light molecules such as LiF. In order to show that this is expected and to make a rough estimate of the relative ease in extracting MBER spectra from the alkali halides, the following calculations were made.

The theoretical beam intensity at the detector can be expressed as[31]

$$I_X = 1.118 \times 10^{22} \frac{p'_X A_s A_d}{\ell^2 (M_X T_X)^{1/2}} \tag{1}$$

where X represents the molecule, A_d is the detector area, A_s the soure slit area, ℓ is the distance from source to detector, p' is the source pressure in mm Hg, M is the molecular weight, and T is the absolute temperature of the source in °K. The source pressure can be expressed as

$$p'_X = 7.321 \times 10^{-20} \frac{T_X}{\lambda' \sigma_X} \tag{2}$$

where σ is the molecular collision cross-section in cm^2 and λ' is the mean free collision path within the source. Combining these two equations one obtains

$$I_X = 818.5 \frac{A_s A_d}{\lambda \ell^2} \frac{1}{\sigma_X} \left(\frac{M_X}{T_X}\right)^{1/2} \tag{3}$$

A reference molecule, LiF, was chosen so that the intensity ratio could be calculated according to Eq. (4).

$$\frac{I_{LiF}}{I_X} = \frac{\sigma_X}{\sigma_{LiF}} \left(\frac{T_{LiF} M_X}{T_X M_{LiF}}\right)^{1/2} \tag{4}$$

Here the assumption is that the mean free path is identical for all molecules at the maximum source pressure producing a stable beam. This is equivalent to assuming the effusive condition in which λ' is approximately equal to the slit width. LiF was chosen as a reference since we found it produced the most intense beam and its spectrum likewise exhibited the greatest signal to noise. The temperature used was obtained experimentally where possible and otherwise estimated from vapor pressure data. The crudest assumption was made in claculating the ratio of collision cross sections. Here σ was assumed to be proportional to the area swept out by a rotor of radius $R = 1/2(r_e + r_A + r_H)$ so that

$$\frac{\sigma_X}{\sigma_{LiF}} = \frac{\left(r_e + r_A + r_H\right)_X^2}{\left(r_e + r_{Li} + r_F\right)^2} \tag{5}$$

where r_A and r_H are the atomic radii of the alkali and halide atoms respectively.

Table XVIII shows these ratios for all the alkali halides along with several other molecular properties such as the velocity, $v_B = 1.22[(2kT)/M]^{1/2}$, where k is the Boltzman constant, and λ_{1000} which is the dimensionless parameter $13\mu/hB$ used for estimating the magnitude of beam deflection. A large λ_{1000} indicates that the (1,0) state will not deflect sufficiently far from the straight through beam. It should be pointed out that Eq. (1) is valid only when the pressure in the molecular beam apparatus is sufficiently low so that no appreciable beam scatter occurs, which is the case when the base pressure is below 10^{-6} mm Hg, and that no collimating slit or similar obstruction intercepts the beam, which is not the case here. However, the effect of a collimating slit will cancel out in the ratios calculated here. It was found that the experimental intensity ratio agreed within ± 20% of that calculated for the eight alkali halides with which the author is familiar.

Table XVIII. Relative detection efficiency calculations for the alkali halide molecules.

X	λ^a_{1000}	v_B (cm/sec)	T_X (°K)	$\frac{\sigma_X}{\sigma_{LiF}}$	$\left[\frac{T_{LiF}}{T_X}\right]^{1/2}$	$\left[\frac{M_X}{M_{LiF}}\right]^{1/2}$	$\frac{I_{LiF}}{I_X}$	Pop. J=1 (%)	Iso. Abund. (%)	Relative Detection Inefficiency
$^{6}Li^{19}F^*$	0.275	9.3	1300	1	1	1	1	0.32	90	1
$^{6}Li^{35}Cl^*$	0.662	6.3	980	1.59	1.15	1.30	2.4	0.19	70	6
$^{6}Li^{79}Br^*$	0.746	4.3	950	1.81	1.17	1.85	3.9	0.15	45	19
$^{6}Li^{127}I^*$	0.950	3.4	923	2.17	1.19	2.31	6.0	0.12	90	16
$^{23}Na^{19}F^*$	1.23	7.2	1300	1.45	1	1.30	1.9	0.067	100	9
$^{23}Na^{35}Cl^*$	2.71	5.5	1065	2.13	1.10	1.54	3.6	0.034	70	49
$^{23}Na^{79}Br^*$	3.98	4.0	1005	2.37	1.14	2.10	5.7	0.023	50	158
$^{23}Na^{127}I^*$	5.22	3.4	965	2.77	1.16	2.45	7.9	0.017	100	149
$^{39}K^{19}F^*$	2.02	5.6	1085	1.91	1.10	1.52	3.2	0.047	93	22
$^{39}K^{35}Cl^*$	5.25	4.7	1020	2.75	1.13	1.74	5.4	0.018	70	137
$^{39}K^{79}Br^*$	8.59	3.7	995	3.03	1.14	2.19	7.6	0.010	47	517
$^{39}K^{127}I$	11.9	3.1	945	3.49	1.17	2.58	9.8	0.007	93	475
$^{85}Rb^{19}F^*$	2.68	4.1	1050	2.11	1.10	2.05	4.8	0.034	72	65
$^{85}Rb^{35}Cl^*$	7.88	3.8	990	3.01	1.14	2.21	7.6	0.011	54	410
$^{85}Rb^{79}Br$	15.2	3.1	980	3.31	1.15	2.58	9.8	0.005	36	1740
$^{85}Rb^{127}I$	23.3	2.8	950	3.80	1.17	2.92	13.0	0.003	72	1980

Table XVIII. (continued)

X	λ^a_{1000}	v_B (cm/sec)	T_X (°K)	$\frac{\sigma_X}{\sigma_{LiF}}$	$\left[\frac{T_{LiF}}{T_X}\right]^{1/2}$	$\left[\frac{M_X}{M_{LiF}}\right]^{1/2}$	$\frac{I_{LiF}}{I_X}$	Pop. J=1 (%)	Iso. Abund. (%)	Relative Detection Inefficiency
$^{133}Cs^{19}F$*	2.82	3.1	1050	2.33	1.10	2.48	6.4	0.029	100	70
$^{133}Cs^{35}Cl$*	9.51	3.0	940	3.31	1.17	2.60	10.1	0.009	75	480
$^{133}Cs^{79}Br$	20.4	2.7	950	3.63	1.16	2.92	12.3	0.003	50	2625
$^{133}Cs^{127}I$	33.5	2.4	940	4.16	1.17	3.22	15.7	0.002	100	2512

*MBER spectra have been observed for these molecules.

[a]Here $\lambda = \mu E/hB$ where the field, E = 13.01, is due to an applied potential of 1000 volts on the dipole deflecting fields, μ is the dipole moment and B is the rotational constant in Hz.

The gross beam intensity is only one of the limiting factors for performing MBER studies on a molecule. Since a single rotational state of a particular isotopic species is selected, one also suffers when the rotational population and isotopic abundance are low. These problems are further aggrivated by splitting of the m_J states by the hyperfine interactions. The estimates of the J = 1, v = 0 state population in the beam, which are also given in Table XVIII, were made from Eq. (6) in which the molecule is considered as a vibrating rotator,[32]

$$\frac{N_{J,v=0}}{N_0} = \frac{hcB}{kT}(2J+1)\exp -\left[\frac{BJ(J+1)hc}{kT}\right]\left(1 - \exp\left[-\frac{\omega_e hc}{kT}\right]\right) \quad (6)$$

The population of the J = 2 state is 67% greater than J = 1, but the population of the (1,±1) and (2,±1) or (2,±2) states are the same, so moving to higher rotational states will not give an increase in intensity in an MBER experiment.

The last column of Table XVIII lists the product of relative intensity, relative population and relative isotopic abundance of the most abundant species. The nuclear spin multiplicity factor was not included since it is somewhat difficult to include in this manner. An assumption implicit in the foregoing calculations is that the efficiency for detection of all the alkali halides on oxygenated tungsten is 100% or at least the same for each. This is certainly true for K, Rb and Cs halides but somewhat tenuous for the Na and Li halides, which would mean that the inefficiency values for the heavier alkali halides may be underestimated.

Of the molecules indicated by the asterisk only KF has not been studied in the spectrometer described earlier. We have found this order of increasing difficulty in obtaining spectra to be borne out by experiment with CsCl and RbCl being the most difficult encountered to date. The large jump from the Rb and Cs chlorides to the bromides indicates that obtaining spectra of the bromides and iodides will be extremely difficult. They have the added undersirable property that λ_{1000} is very large in addition to possessing large nuclear spins. These molecules are most interesting from the theoretical point of view since they are composed of the most polarizable ions, which means that their dipole moment are the most sensitive in the model to be described in the next section.

V. POLARIZABLE ION MODEL FOR THE ALKALI HALIDE MOLECULES

I. Introduction

Over the past forty years a number of attempts have been made to correlate dissociation energies and dipole moments of the alkali halides in ionic models. The first models were rather simple versions[35,36] which were adequate for the scanty experimental data available at the time. As more data became available more complex models were examined. For example, Rittner[37] followed Debye's[38] approach in that he considered the ions as polarizable. He used Pauling's polarizabilities[39] and the experimental spectroscopic constants available to calculate dissociation energies and electric dipole moments. The agreement with experimentally measured values was good; however, these experimental values were in many cases inaccurate or incomplete. Then Honig et al.[29] added to Rittner's model a calculation of the second Dunham coefficient, a_1.[41] They found the agreement to be not very good for many of the alkali halides. When more and better experimental data were available, Klemperer et al.[42,43,44] found that this model would not predict the dipole moments with good agreement with the experimental values. Among the variations which they employed was a consideration of the electrostatic term of the potential energy as, first, that from a point charge or $\phi = - e^2/r$ which resulted in reasonable W_e and a_1 values but poor μ values which required polarizability considerations like Rittner had used, and second, that due to dipole plus higher polarizabilities through the use of a spherical conductor model in the electrostatic potential calculations. However, the inclusion of higher polarizations destroyed the agreement of the a_1 values which had existed when only the dipole polarization was included.

Recently, K. Street, Jr. and C. Hollowell[18] have modified this polarizable ion model by including several effects previously neglected and by determining the multipole polarizabilities in a fashion which appears to be much more reasonable than that used by Klemperer et al. who forced the dipole moments to fit the experimental data in order to obtain polarizability values for calculation of W_e and a_1. The present work is a continuation of this examination begun by Street and Hollowell and

uses what should be a somewhat better set of free ion polarizabilities and variation of polarizability with internuclear distance as well as inclusion of terms in the dipole moment which arise from the fields produced by multipole polarizations. As in the previous work, values for the dissociation energy, W_e, the Dunham coefficient in the potential energy function, a_1, the dipole moment, μ, and its vibrational variation, μ_I, are calculated and compared with a more complete set of experimental data for the alkali halides.

B. Polarizability Calculations

The method of determining the polarizabilities here is basically the same as described by Hollowell.[18] The variation of polarizability with internuclear separation is determined by an equation of simple form which represents as closely as possible Burns'[47] calculated quadrupole, octupole and hexadececapole polarizabilities for the alkali halides at r_e, the equilibrium internuclear distance. In most cases these values are smaller than the free ion values. The equation represents the increase in polarizability to the limit of the free ion value at a finite value of the internuclear separation, r. Since the quadrupole and higher polarizabilities have a major contribution in the outer parts of the electron distribution, the value of r where $\alpha = \alpha_{inf}$ increases as one moves to higher polarizabilities.

The alkali dipole polarizabilities were taken to be:

$$\alpha_A^1 = \alpha_A^1(\text{free ion}) \qquad \text{or} \qquad \alpha_{inf}$$

while the halide dipole polarizabilities had the following form:

$$\alpha_H^1 = \alpha_H^1(\text{free ion})\ \sin^{3/2}\left(\frac{\pi r}{2Fr_o}\right)$$

where F = 2.4, 2.2, 2.1, and 2.1 for F^-, Cl^-, Br^-, and I^- respectively. It should be pointed out here that the halide dipole polarizabilities only follow the form of those calculated by Burns which are too low since

he considered the s-p and p-s contributions to cancel. Sternheimer[48] has shown this is not true for the halides. Here the hydrogen halides and free ion values were used to obtain the F values for the above equation.

Burns included all terms in calculating the higher polarizabilities so that they should be more representative of the actual values. This data was fitted by the following equations:

$$\alpha_A^{\ell}(r) = \alpha_A^{\ell}(\text{free ion}) \sin^{2\ell}\left(\frac{\pi r}{\left[\frac{21+2\ell}{5}\right] r_o}\right) \tag{7}$$

$$\alpha_H^{\ell}(r) = \alpha_H^{\ell}(\text{free ion}) \sin^{2\ell}\left(\frac{\pi r}{[F+0.4(\ell-2)] r_o}\right) \tag{8}$$

$$F(F^-) = 2.9 \qquad F(Cl^-) = 2.6 \qquad F(Br^-, I^-) = 2.4$$

These are the polarizabilities at r where $\ell = 2,3,4$, and 5 represent the quadrupole, etc. polarizabilities, r_o is Pauling's[46] crystal radius and $\alpha_{A,H}^{\ell}$(free ion) are the free ion polarizability values. The free ion polarizabilities used here are from a consistent set[49] of dipole polarizabilities obtained by a semi-emperical extrapolation of positive ion polarizabilities (estimated from spectroscopic data). They are only slightly different from those used by Hollowell. The values employed here are:

ion	α_A^{ℓ}(free ion) Å^3	ion	α_H^{ℓ}(free ion) Å^3
Li^+	0.028	F^-	1.62
Na^+	0.148	Cl^-	5.10
K^+	0.811	Br^-	6.60
Rb^+	1.350	I^-	10.10
Cs^+	2.250		

The higher or ℓ-pole free ion polarizabilities were calculated from these dipole values according to a slightly modified spherical conductor model where,

$$\alpha_X^{\ell}(\text{free ion}) = \kappa^{\ell-2} \frac{a^{2+1}}{\ell!}$$

in which a is the radius of the spherical conductor for $\ell = 1$, and

$\kappa(A^+) = 0.7$ $\kappa(F^-) = 1.3$

$\kappa(Cl^-, Br^-, I^-) = 0.7$

C. Dissociation Energy Calculations

Following the same form as in previous models, the potential energy is expressed as:

$$W = \phi_E + \phi_{Rep} - c/r^6 \tag{9}$$

in which ϕ_E is the electrostatic contribution, ϕ_{Rep} is the repulsion terms and c/r^6 is the Van der Waal's term. Here ϕ_E contains all the terms arising from the multipole electrostatic interactions of the two ions. Since the treatment is identical to that described by Hollowell we will not go into detail here concerning the derivation of the final equations used to compute the electrostatic potential energy.

The ℓ-pole moments are computed through the solution of the simultaneous equations:

$$P_A^{(\ell)} = \alpha_A^{\ell}\left[-\frac{e\ell!}{r^{\ell-1}} + \sum_{m=1} \frac{P_H^{(m)}}{r^{m+\ell+1}} \frac{(m+\ell)!}{m!}\right] \tag{10}$$

$$P_H^{(m)} = \alpha_H^{m}\left[-\frac{em!}{r^{m+1}} + \sum_{\ell=1} \frac{P_A^{(\ell)}}{r^{m+\ell+1}} \frac{(m+\ell)!}{\ell!}\right] \tag{11}$$

in which m and ℓ take the values 1,2,...5 since higher multipole moments give insignificant contributions. The electrostatic potential energy of the ions is thus described as follows:

$$\phi_E = \frac{e^2}{r_e} - \int_{\infty}^{r_e}\left(\sum_{\ell=1} \frac{P_A^{(\ell)}(\ell+1)}{r^{+2}} + \sum_{m=1} \frac{P_H^{(m)}(m+1)}{r^{m+2}}\right)$$
$$+ \int_{\infty}^{r_e} \sum_{\ell=1} \sum_{m=1} \frac{P_A^{(\ell)} P_H^{(m)}}{r^{\ell+m+2}} \frac{(\ell+m+1)!}{\ell!\ m!}$$

in which the polarizabilities discussed earlier are used.

The repulsion term is simply $Ar^{-2}e^{-r/\rho}$. The values of A and ρ are determined through the relationships

$$\left(\frac{dW}{dr}\right)_{r=r_e} = 0 \qquad \text{and} \qquad \left(\frac{d^2W}{dr^2}\right)_{r=r_e} = k$$

where the force constant, k, is derived from the vibrational frequency, ν_o, according to:

$$\nu_o = \frac{1}{2\pi}\left(\frac{k}{\mu_A}\right)^{1/2}$$

where μ_A is the reduced mass.

The Van der Waal's attractive force constant is determined by the relation:[50]

$$c = \frac{3}{2}\alpha_A^1 \alpha_H^1 \frac{I_A^{(II)}(-E_H')}{I_A^{(II)} - E_H'}$$

in which $I_A^{(II)}$ is the second ionization potential[51] of the alkali atom and E_H' is the electron affinity[52] of the halogen atom.

The dissociation energy, W_e, is then calculated from Eq. (9) and compared with the experimental value obtained from the following:

$$W_e = D_o + I_A^{(I)} - E_H' + 1/2h\nu_o$$

in which D_o is the dissociation energy[53] into neutral atoms and $I_A^{(I)}$ is the first ionization potential[51] of the alkali atom. These values are tabulated from comparison in Table IXX. In the same table are listed the calculated and observed a_1 values. These are computed from Eqs. (12) and (13) below:

$$a_1(\text{calc.}) = \frac{r_e^3 W'''(r_e)}{3!\left(\frac{k\, r_e^2}{2}\right)} \tag{12}$$

and

$$a_1(\text{expt.}) = \frac{-\alpha_e\, \omega_e}{6\, B_e^2} - 1 \tag{13}$$

Table IXX. The calculated and experimental values of W_e and a_1 for the alkali halides.

	W_e(calc.)	W_e(expt.)[a]	Δ	a_1(calc.)	a_1(expt.)	Δ
LiF	-7.944	-7.930	-0.014	-2.538	-2.701[b,c]	0.163
LiCl	-6.533	-6.560	0.027	-2.672	-2.721[d]	0.049
LiBr	-6.144	-6.380	0.236	-2.704	-2.718[e,f,g]	0.014
LiI	-5.729	-5.990	0.261	-2.743	-2.730[e,g,h]	-0.013
NaF	-6.651	-6.640	-0.011	-2.935	-3.133[j,k,l]	0.199
NaCl	-5.661	-5.650	-0.011	-2.974	-3.076[m]	0.102
NaBr	-5.376	-5.530	0.154	-2.979	-3.046[e]	0.067
NaI	-5.066	-5.220	0.154	-2.982	-3.016[e]	0.034
KF	-5.923	-5.990	0.067	-3.067	-3.116[n]	0.049
KCl	-4.987	-5.040	0.053	-3.232	-3.226[m]	-0.005
KBr	-4.743	-4.890	0.147	-3.126	-3.242[e,o]	0.116
KI	-4.464	-4.580	0.116	-3.169	-3.246[e]	0.078
RbF	-5.693	-5.770	0.077	-3.140	-3.135[n]	-0.005
RbCl	-4.761	-4.810	0.049	-3.388	-3.297[m]	-0.091
RbBr	-4.537	-4.720	0.183	-3.397	-3.326[e]	-0.072
RbI	-4.272	-4.430	0.158	-3.223	-3.344[e]	0.121
CsF	-5.519	-5.640	0.121	-3.128	-3.032[n]	-0.096
CsCl	-4.535	-4.770	0.235	-3.593	-3.319[m]	-0.274
CsBr	-4.315	-4.710	0.395	-3.647	-3.377[e]	-0.270
CsI	-4.068	-4.410	0.342	-3.670	-3.429[e]	-0.241

[a]Ref. 53 [c]Ref. 55 [e]Ref. 57 [g]Ref. 59 [j]Ref. 60 [l]Ref. 62 [n]Ref. 23
[b]Ref. 54 [d]Ref. 56 [f]Ref. 58 [h]Ref. 9 [k]Ref. 61 [m]Ref. 63 [o]Ref. 64

where $W'''(r_e)$ is the third derivative of the potential energy. It should be noted that the agreement of the calculated and observed values of the heavier alkali halides is much better than Hollowell achieved with different polarizability values.

D. Dipole Moment Calculation

Previous calculations of the molecular electric dipole moment have all been based on Debye's[38] approach for the hydrogen halides. Rittner[37] considered the dipole moment as a sum of the terms due to charge separation and the induced moments on each ion arising from the dipole polarizability of the ions. This representation is described by the following equations and sketch:

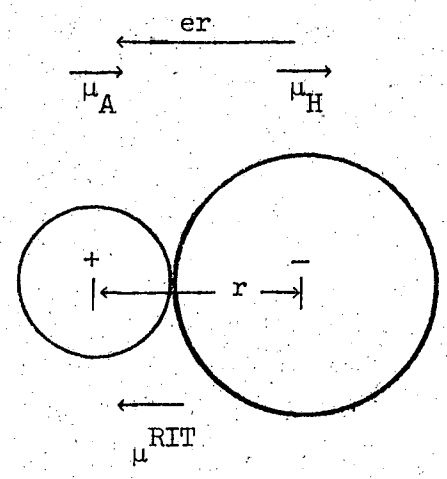

$$\mu^{RIT} = er - \mu_A - \mu_H$$

$$\mu^{RIT} = er - \left(\frac{r^4 e(\alpha_A^1 + \alpha_H^1) + 4\, re\, \alpha_A^1 \alpha_H^1}{r^6 - 4\, \alpha_A^1 \alpha_H^1} \right)$$

where μ_A and μ_H are the moments induced on the alkali and halide ions respectively. This interpretation predicts dipole moments which are 15-25% lower than the experimental values.

Hollowell[18] has gone one step further and included a term which represents the repulsion induced dipole moment that results from the redistribution of electron density in the inter-ion region. He considered the repulsion force on the halide to be:

$$f = - E_h q_h$$

in which E_h is the field at the halide kernel (halide ion less the eight valence electrons) of charge $q_h = +7e$. This field arises from the repulsive interaction which causes a redistribution of electron density between the ions. Since the halide ions are much more polarizable than the alkali ions, this change in electron distribution would be expected to occur mostly on the halide ion. A sketch of how these interactions affect the dipole moments is:

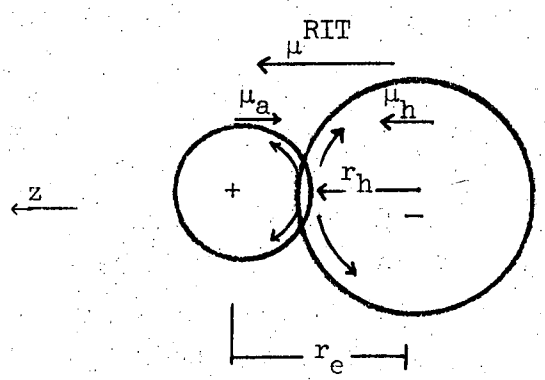

where μ_a and μ_h are the repulsion induced dipole moments. They are evaluated from the following considerations. Consider only the outer electrons of the halide ion which varies in charge density in such a manner that the field in the z direction can be expressed

$$\delta E_z = \frac{\delta q_z}{r_h^2} = \frac{\delta q \cos \theta}{r_h^2}$$

where r_h is the effective distance of the changing electron density, δq, from the core and θ represents the angle between the vector r_h and the z-axis.

$$\delta\mu = \delta q \; r_h \cos\theta$$

so $$\frac{\delta\mu}{\delta E} = r_h^3$$

and $$\mu_h = r_h^3 \, E_h^e \quad .$$

The field E_h at the halide core produced by repulsion effects will thus be due to E_h^e plus the field produced by the small repulsion dipole moment μ_a of the alkali ion. Moments produced by higher order multipole terms are small and thus neglected. This field may be written:

$$E_h = \frac{\mu_h}{r_h^3} - \frac{2\mu_a}{r_e^3} \tag{14}$$

Here r_h is expressed as a function of the alkali halide internuclear separation, i.e. $r_h = \gamma r_e$ where γ is a scaling factor of the internuclear distance, r_e. Since μ_a should be smaller than μ_h in proprotion to the respective dipole polarizabilities, the following relation is introduced:

$$\mu_a = \beta\left(\frac{\alpha_A^1}{\alpha_H^1}\right) \mu_h \quad .$$

Combining these equations, one obtains for the total repulsion dipole moment

$$\mu^{REP} = \mu_h - \mu_a = \frac{f}{q_h} \gamma^3 \, r_e^3 \; \frac{\left[1-\beta\left(\frac{\alpha_A^1}{\alpha_H^1}\right)\right]}{\left[1+2\gamma^3\beta\left(\frac{\alpha_A^1}{\alpha_H^1}\right)\right]} \tag{15}$$

The total equilibrium dipole moment can be then expressed as:

$$\mu_e = \mu_e^{RIT} + \mu_e^{REP}$$

and compared with the experimental values which have been expressed in the form:

$$\mu_v = \mu_e + \mu_I(v + 1/2)$$

where v is the vibrational state and μ_I is the vibrational variation of the moment. The theoretical or calculated μ_I values come from an anharmonic oscillator approximation of the vibrational motion (see Ref. 18) which results in:

$$\langle\mu\rangle_v = \mu_e + \left[-3a_1 \frac{B_e}{\omega_e} \left(\frac{d\mu}{d\xi}\right)_{\xi=0} + \frac{B_e}{\omega_e} \left(\frac{d^2\mu}{d\xi^2}\right)_{\xi=0} \right] (v + 1/2) \qquad (16)$$

Here $\xi = (r-r_e)/r_e$ and the term in brackets is the calculated μ_I.

In the present work an expansion on the Rittner portion of the dipole moment and its vibrational variation has been performed. Here we have included the contributions of the quadrupole and higher multipole polarizations to the fields producing the dipole moment. So instead of calculating μ_A and μ_H as previous workers have done, we have used the fact that $P_A^{(1)}$ and $P_H^{(1)}$ are determined by the solution of the simultaneous Eqs. (10) and (11). Since the field at nuclear H is:

$$E_H = \sum_0^{\ell} \frac{(\ell+1)\, P_A^{(\ell)}}{r^{\ell+2}} \qquad (17)$$

and similarly for nucleus A (substitute A for H), the dipole moment due to considering terms up to $\ell = 5$ is, thus:

$$\mu_H = P_H^{(1)} = \alpha_H^{(1)} \sum_0^5 \frac{(\ell+1)\, P_A^{(\ell)}}{r^{\ell+2}} \qquad (18)$$

$$\mu_A = P_A^{(1)} = \alpha_A^{(1)} \sum_0^5 \frac{(\ell+1)\, P_H^{(\ell)}}{r^{\ell+2}} \qquad (19)$$

The total dipole moment can thus be expressed:

$$\mu_e = \mu^{POL} + \mu^{REP}$$

$$\mu_e = er_e - (\mu_A + \mu_H) + \mu^{REP}$$

$$\mu_e = er_e - P_A^{(1)} - P_H^{(1)} + \mu^{REP}$$

Similarly, the μ_I value are calculated by taking the appropriate derivatives of Eqs. (18) and (19) above and then substituting into Eq. (16). So μ_I can be expressed as:

$$\mu_I = \mu_I^{POL} + \mu_I^{REP} \quad .$$

Table XX lists the calculated and observed μ_e and μ_I values as well as the values calculated by Hollowell. Here the best fit was obtained with $\gamma = 0.77$ and $\beta = 0.12$. The agreement is quite good, especially considering the disagreement Klemperer et al. obtained when adding the multipole polarizations to their model. The present dipole moment results agree with experimental values as well as did those calculated by Hollowell, while the W_e and a_1 results from the model here are in better agreement than were those in the earlier work.

There are certainly some weak points in this model, especially in regard to the repulsive interactions, and the model is certainly not unique. The variation of the polarizabilities with internuclear distance is only a plausible estimate. However, the agreement obtained here is encouraging in that a completely ionic model, which includes (although in a very over simplified manner) all the major effects expected, gives a quite good account of the alkali halides.

Table XX. The calculated and experimental dipole moments of the alkali halide molecules.

	u_e^{POL}	u_e^{REP}	u_e(calc.)	u_e(expt.)	u_e(Ref.18)	u_I^{POL}	u_I^{REP}	u_I(calc.)	u_I(expt.)
LiF	5.547	0.803	6.350	6.284[a]	6.292	0.0916	-.0150	0.0765	0.0815[a]
LiCl	5.743	1.310	7.053	7.085[a]	6.981	0.0980	-.0203	0.0777	0.0814[a]
LiBr	5.524	1.562	7.086	7.226[b]	7.176	0.0992	-.0221	0.0771	0.0775[b]
LiI	5.402	1.871	7.274	7.387[c]	7.403	0.1028	-.0245	0.0783	0.0776[c]
NaF	7.350	0.907	8.257	8.123[d]	8.098	0.0751	-.0140	0.0610	0.0644[d]
NaCl	7.640	1.401	9.041	8.972[e]	8.946	0.0722	-.0162	0.0560	0.0595[e]
NaBr	7.493	1.637	9.130	9.092[e]	9.135	0.0676	-.0160	0.0516	0.0530[e]
NaI	7.369	1.939	9.308	9.210[f]	9.347	0.0673	-.0169	0.0504	0.0507[f]
KF	7.545	1.132	8.676	8.550[g]	8.555	0.0824	-.0160	0.0665	0.0690[g]
KCl	8.410	1.755	10.165	10.239[a]	10.242	0.0778	-.0193	0.0585	0.0600[a]
KBr	8.441	2.020	10.461	10.603[h]	10.633	0.0648	-.0168	0.0479	0.0502[h]
KI	8.531	2.329	10.860		11.105	0.0638	-.0175	0.0463	
RbF	7.309	1.238	8.546	8.513[f]	8.454	0.0824	-.0158	0.0665	0.0665[f]
RbCl	8.401	1.989	10.483[f]	10.483[f]	10.519	0.0757	-.0197	0.0560	0.054[f]
RbBr	8.478	2.297	10.775		11.013	0.0617	-.0171	0.0447	
RbI	8.632	2.630	11.263		11.632	0.0518	-.0148	0.0370	
CsF	6.337	1.392	7.729	7.849[f]	7.791	0.0888	-.0163	0.0725	0.0704[f]
CsCl	7.926	2.381	10.307	10.358[f]	10.508	0.0854	-.0236	0.0618	0.058[f]
CsBr	8.066	2.784	10.850		11.174	0.0680	-.0201	0.0479	
CsI	8.346	3.155	11.501		12.048	0.0608	-.0190	0.0418	

[a]Ref. 45 [c]Ref. 9 [e]Ref. 40 [g]Ref. 33
[b]Ref. 58 [d]Ref. 61 [f]Present work [h]Ref. 85

ACKNOWLEDGMENTS

I am grateful to Professor Kennth Street, Jr. for his immaginative guidance, and for his patience, interest and encouragement throughout this work.

It has also been my good fortune to have enjoyed a close association with Dr. Alvin J. Hebert. His optimism in the face of difficulties was a constant source of encouragement and our many discussions on a wide range of topics I found to be quite enlightening. I would also like to express my appreciation to the other members of the molecular beam group for their helpful assistance.

The work was performed under the auspices of the U. S. Atomic Energy Commission.

APPENDICIES

A. Molecular Beam Detection Studies

1. Introduction

As was mentioned previously, one of the prime limitations of the MBER technique is the detection of molecular beams. The most useful method of detection of molecules containing atoms with relatively low ionization potentials is surface ionization on hot tungsten. More specifically, MBER studies of only the alkali halides, BaO[65], SrO[66], and Tl halides have been reported primarily because of this limitation in detection efficiency for elements possessing high ionization potentials (Table A-I shows ionization potentials of a number of elements). Some experiments which utilize both polycrystaline and single crystal tungsten filaments were performed in order to determine the usefulness of a single crystal as a MBER detector.

A number of other beam detection techniques have been employed for MBER studies, e.g. the outdated Pirani gauge and the more recent innovation of electron bombardment. The electron bombardment technique holds the most promise as a general purpose detector, although a highly efficient ionizer of this type has not been developed yet. The only molecule which has been studied through the use of such an ionizer is HF.[12] This molecule, being a gas and having little hyperfine splitting, has the advantage of larger populations in the low rotational states than do condensible molecules which require high temperatures to produce a beam, such as the oxides and sulfides of the alkaline earth and transition metals. Auger detection has also been used in the study of metastable excited states with molecular beam techniques,[10,67] however this method is not applicable to detection of low energy beams of ground state molecules which are produced in normal MBER sources.

Work on another type of general purpose ionizing detector, which uses a microwave produced gaseous discharge, has also been performed and is discussed later in this section. Although this so-called "plasma" detector did not function as a detector; it has potential as an ion or excited state source for other fields of investigation.

Table A-I. Ionization potentials and electronegativaties of a number of elements.

Element	Ionization Potential[77] I	Ionization Potential[77] II	Electronegativity[46]
Cs*	3.87 eV	23.4 eV	0.7
Rb*	4.159	27.36	0.8
K*	4.318	31.66	0.8
Na*	5.12	47.06	0.9
Ba*	5.19	9.95	0.9
Ra	5.252	10.099	0.9
Li*	5.363	75.26	1.0
La	5.6	11.4	1.1
Sr*	5.667	10.98	1.1
In	5.76	18.79	1.7
Al	5.96	18.74	1.5
Ga	5.97	20.43	1.6
Tl*	6.07	20.32	1.3
Ca	6.09	11.82	1.0
Sn	7.30	14.5	1.8
Pb	7.38	14.96	1.8
Mn	7.41	15.70	1.5
Ag	7.542	21.4	1.9
Co	7.81	17.3	1.8
Fe	7.83	16.16	1.8
W	8.1		1.7
Si	8.12	16.27	1.8
Cd	8.96	16.84	1.7
Zn	9.36	17.89	1.6
Se	9.70	21.3	2.4
Hg	10.39	18.65	1.9
I	10.6	19.4	2.5
Br	11.80	19.1	2.8
Xe	12.08	21.1	-
Cl	12.952	23.67	3.0
O	13.55	34.93	3.5
Kr	13.93	26.4	-
Ar	15.68	27.76	-
F	17.34	34.81	4.0
Ne	21.47	40.9	-
He	24.46	54.14	-

*Molecules containing these elements have been successfully detected by surface ionization on tungsten in MBER experiments.

2. Surface Ionization on Tungsten

Considerable research has been performed in the field of ionization on hot metal surfaces since the production of positive ions by surface ionization was first reported in 1923.[68,69] The most up to date review article of the author's acquaintance which covers both positive and negative surface ionization is that of Zandberg and Ionov.[70]

In his thesis, Werning[71] points out some of the reasons which explain deviation from Saha-Langmuir theory which various authors have reported. In high work quantitative agreement with the theory is obtained under conditions of moderate ultra high vacuum (5×10^{-9} mm Hg) and very high temperatures where interferring mechanisms are not important. He finds that most deviations from the Saha-Langmuir theory can be explained as due to chemical reactions between the ionizing species being studied and the large quantities of impurities in well aged filaments of tungsten, tantalum and rhenium. In some cases discrepancies are due to vacuum insufficient to reduce oxygen or fluorine sources below the interference level.

Our interest here was not to investigate work functions of ionizing surfaces or the agreement of Saha-Langmuir theory with experiment, but rather to determine the behavior and efficiency of tungsten at various temperatures and oxygen pressures in high vacuum (5×10^{-7} mm Hg) with the objective of molecular beam detection for MBER experiments. For this reason no special vacuum or ion accelerator and collector equipment were constructed; the MBER apparatus described earlier was used with polycrystaline and 110 surface of single crystal tungsten[72] serving as detectors.

Equations (1)-(4) in Table A-II show the dependence of ionization on the surface work function, ϕ, the atomic ionization potential, I, and the surface temperature, T, as predicted from Saha-Langmuir theory. As is well known, oxygenated tungsten has a higher work function than the unoxygenated surface. Table A-III lists measurements of the work function of oxygenated polycrystaline tungsten found in the literature. The basic premise of the present work is derived from this fact. Since a substance of high electronegativity such as flourine or oxygen (see Table A-I) which

Table A-II. Equations describing ideal surface ionization behavior.

Saha-Langmuir Eq.

$$\frac{i_{ion}}{i_{atom}} = \frac{\omega_i (120\ T^2)}{\omega_a\ J_{sat}} \exp\left[\frac{-eI}{kT}\right] \tag{1}$$

Richardson Eq.

$$J_{sat} = AT^2 \exp\left[\frac{-e\phi}{kT}\right] \tag{2}$$

Langmuir-Kingdon Eq.

$$\frac{i_{ion}}{i_{atom}} = \frac{\omega_i}{\omega_a} \exp\left[\frac{e(\phi - I)}{kT}\right] \tag{3}$$

Fraction of particles leaving surface as ions:

$$\beta = \frac{n_+}{n_+ + n_o} = \left(1 + \frac{\omega_i}{\omega_a} \exp\left[\frac{I - \phi}{kT}\right]\right)^{-1} \tag{4}$$

i = ion or atom current

ω = stastical weight

J_{sat} = electron current density at saturation

T = temperature (°K)

I = atomic ionization potential (eV)

ϕ = surface work function (eV)

n_+ = number of positive ions emitted by surface

n_o = number of atoms emitted by surface

Table A-III. The variation of the work function of oxygenated polycrystaline tungsten with temperature as reported by Haque and Donaldson.[84]

Temperature (°K)	Work Function (eV)
303	6.82
781	6.80
1133	6.65
1298	6.22
1503	6.16
1649	5.84
1795	4.95
2000	4.80
2073	4.70
2273	4.68

has reacted with polycrystaline tungsten causes an increase in work function and vice versa for substances of electronegativity lower than tungsten's, it was felt that by starting with a surface of higher work function than non-oxygenated polycrystaline tungsten one might obtain a work function for the oxygenated surface which is significantly larger than that of the oxygenated polycrystaline tungsten. Table A-IV shows the values of the work functions of various crystal planes of single crystal tungsten which have been reported in the literature.

A number of runs were made which used five standard polycrystaline filaments with ^{87}Sr and ^{7}Li as beam material and a base pressure of about 4×10^{-7} mm Hg in the detector chamber. In some runs oxygen was directed on the filament through a variable leak. Very slight increase in intensity (less than a factor of 2) occurred up to about 1×10^{-6} mm Hg at which point the intensity would decrease due to substantial beam scatter. Figure 10 shows the variation of ion intensity with the inverse of the surface temperature for the average Sr and Li experiment. The same type curve was obtained for oxygenated tungsten, but shifted slightly along the ordinate. Surface temperatures were measured by means of a Pyro Micro-Optical Pyrometer which had been calibrated against a standard tungsten ribbon filament lamp. Runs were made by increasing and decreasing filament temperature with the same behavior resulting in each case.

Similar experiments were performed with a single crystal filament with the 110 surface exposed.[72] The results are shown in Figs. 11 and 12. As one would expect the high temperature portion of the curves for the two filament types are quite different since the non-oxygenated surface work functions of polycrystaline and 110 single crystaline tungsten differ by about 1 eV. The three relative maxima observed with ^{7}Li on 110 tungsten agree with similar observations by Weierhausen[73] on oxygenated polycrystaline tungsten. He explains the behavior on the basis of three types of adsorption center and calculates adsorption energies of 4.5, 3.1, and 1.7 eV, respectively. A careful comparison of his work with the mass spectrometric study of the oxidation of tungsten by Schissel and Trulson[74] indicates that the three sites are composed of W_2O_6, WO_3 and WO_2 respectively, since these are the predominant ionic species emitted at the

Table A-IV. Some measured work functions of several crystal orientations for tungsten. All values are given in electron volts.

Method	Ref.	(110)	(112)	(111)	(116)	(100)
Field Emission	78	5.7-	4.65-	4.39	4.30	
Surface Ionization	79	5.41(4)		4.49(4)		
Thermionic Emission	80	4.72	4.65	4.38	4.29	4.52
	81	5.22(1)		4.74(14)		
	82	5.30				4.66
	83	5.33				4.65

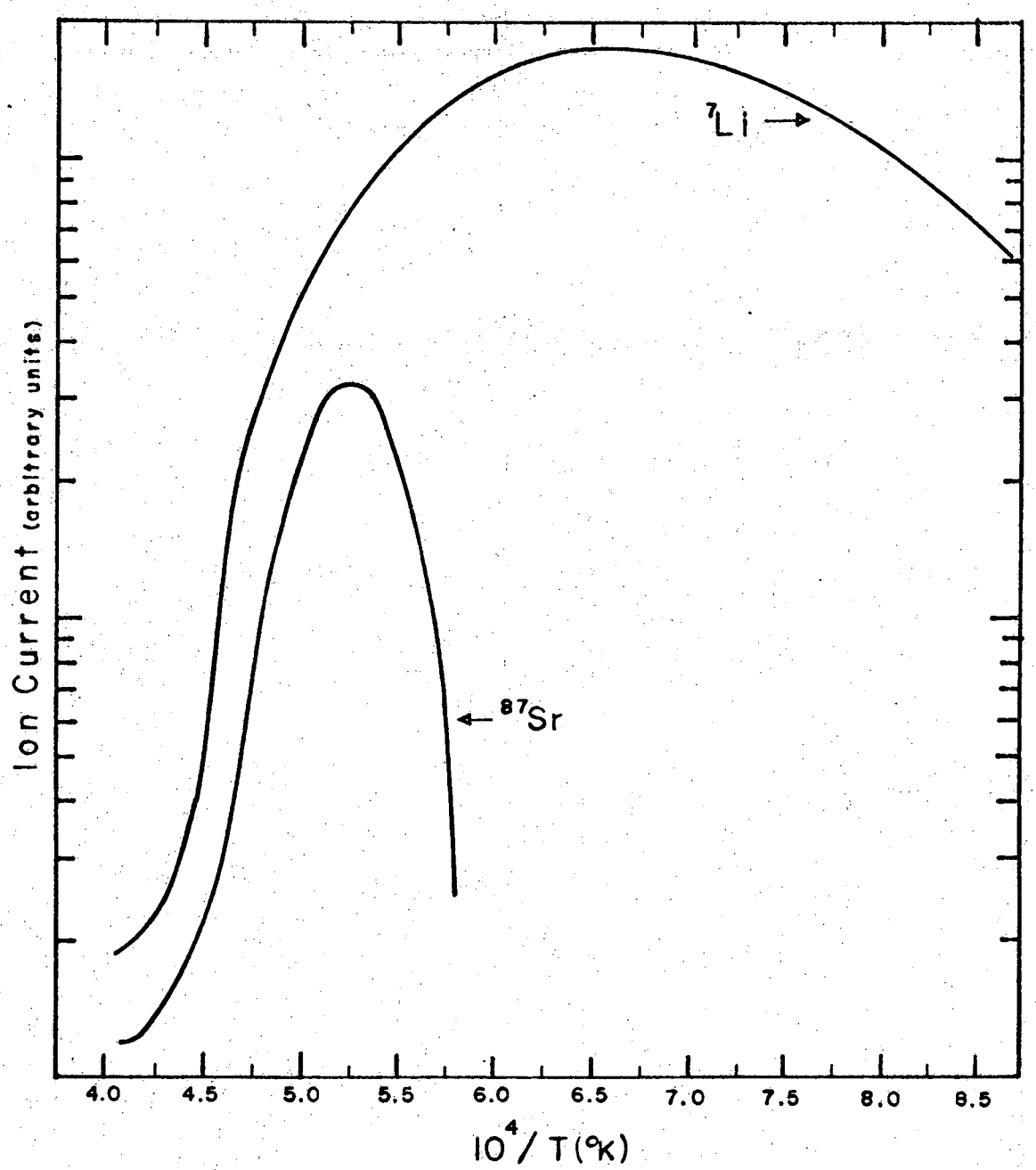

XBL 6711-6037

Fig. 10. The observed $^{87}Sr^+$ and $^7Li^+$ current produced by a polycrystalline tungsten surface between 1000 °K and 2500 °K.

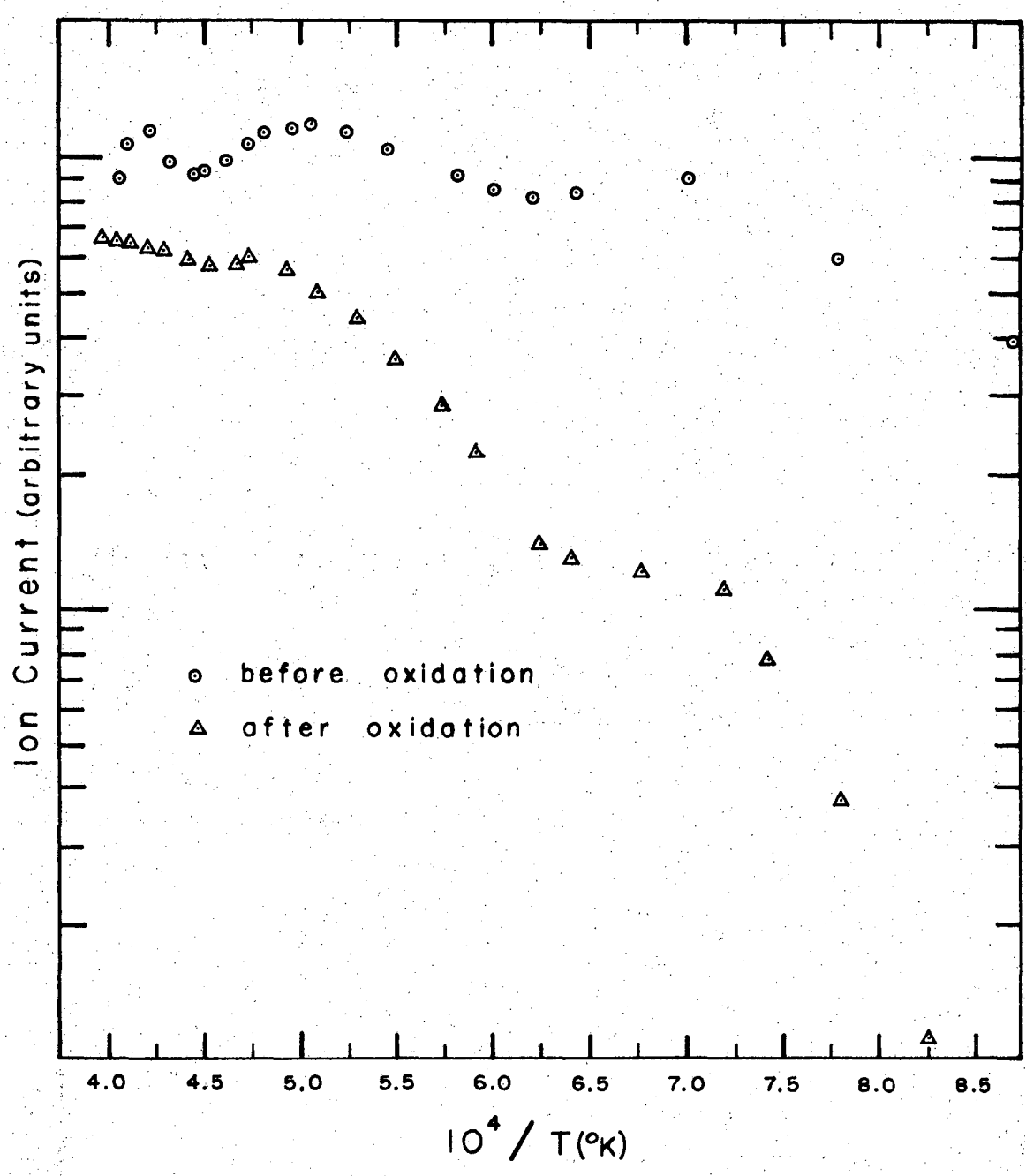

XBL 6711-6036

Fig. 11. The $^{7}Li^{+}$ current from the (110) tungsten surface both before and after filament oxidation.

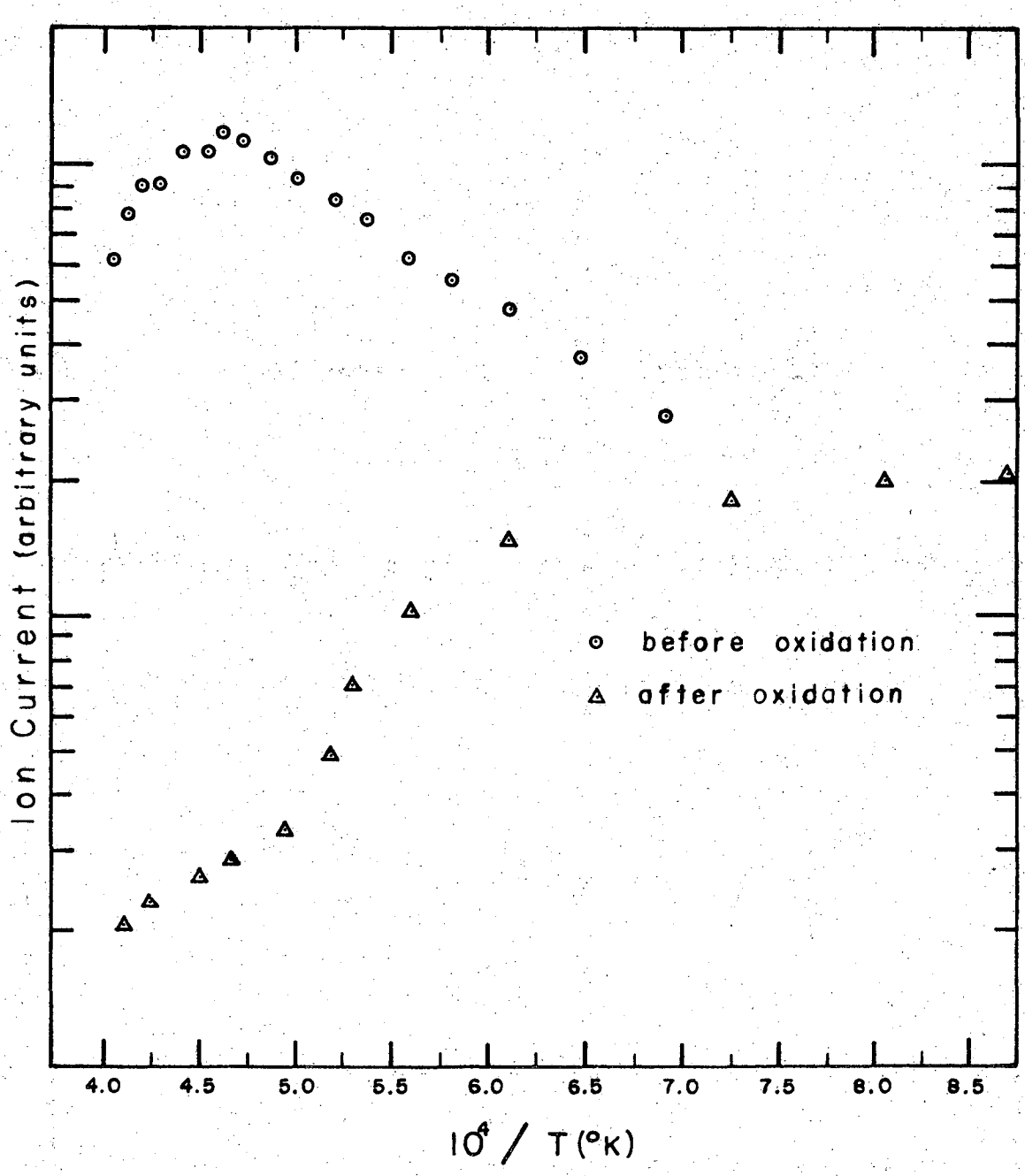

XBL 6711-6035

Fig. 12. The $^{87}Sr^{+}$ current from the (110) tungsten surface both before and after filament oxidation.

corresponding temperatures. This behavior was not observed for the polycrystaline filaments used in the present work. We can account for this discrepancy only by assuming the filaments used here had not recrystalized as uniformly as did Weierhausen's. A truly multicrystaline surface would average the effect out to give smooth curves like those observed. The 110 filament showed somewhat different behavior after it had been treated with O_2 than before oxygenation. This is especially noticed in the low temperature region where improved response characteristics were observed but ionization was less than at very high temperatures. A good explaination for this is lacking.

The behavior of all filaments above 2000°K was contrary to what is expected from the Saha-Langmuir theory, i.e. a negative slope should be obtained when ion current is plotted against 1/T (see Reynold's study of Sr on 110 tungsten[79]). This is to be expected considering the ambient pressure in the detector chember. One might argue that elements with higher ionization potentials should have been used in this study for more dramatic effects. This would have been desirable had beam intensity and stability not been somewhat of a problem even with the elements used since the beam source was about 1 meter from the detector resulting in a loss in intensity of about 100-1000 times compared to other surface ionization studies. In fact, for this reason it was impossible to estimate the relative efficiencies of the two types of filaments used here, as was desired at the outset.

Oxygenation of the 110 filament did not produce the factor of 10 improvement in detection efficiency relative to oxygenated polycrystaline tungsten as was expected, but on the contrary, showed a degradation of the uniform efficiency observed previous to oxygenation. This change in behavior after oxygenation might be due to etching of the surface in such a manner that planes other than 110 are exposed. This possibility has been suggested by Fred Reynolds[75] who noticed significant changes in the Laue patterns for 110 filaments heated in "poor" vacuum of about 1×10^{-6} mm Hg; thus, exposure of other crystal planes is indicated. Since the 110 filament showed evidence of better efficiency than the polycrystaline one at high temperatures, it would be useful when working

with elements which normally exhibit poor response characteristics at moderate filament temperatures (below 1600°K) such as La, Sr, and Al. However, operation of such a filament at pressures of 10^{-6} - 10^{-7} mm Hg might result in a very short effective life of the 110 surface, especially if a large fraction of the residual gas is oxygen.

3. Microwave Discharge Ionization

Microwave discharge cavities have been used fairly extensively as excitation sources for studying atomic spectra of gaseous elements or of condensable elements through vaporization of the substance by heat from the discharge gas. It is well established that metastable and ionic species can be produced in a static gaseous system without undue heating, the need for electrodes or for high voltages in microwave produced discharges. A number of cavities used for these studies have been designed by Broida et al.[76] who made a study of the operating characteristics of cavities with various shapes.

Since these sources can produce highly ionized species, we felt that they might serve as a molecular beam ionizer if the discharge could be operated in vacuum of the order of 10^{-6} mm Hg. In order to try this technique as a beam ionizer we chose the most versital and efficient of the cavities described by Broida et al. as a discharge source. We determined that a stable discharge could be maintained in a dynamic system, i.e. continuous mechanical pumping on the discharge tube while maintaining a pressure of about 50 to 100 μ Hg via a gas leak. Since this initial experiment was successful, we decided to adapt this cavity so that it could be operated while completely enclosed in a vacuum envelope.

The cavity was number 5 in Broida's work and the discharge tube used here consisted of sealed concentric quartz tubing of 13 mm and 9 mm O.D. (see Fig. 13). The space between the two tubes was open to the outside and used to introduce cooling air while the inner tube was open to a variable leak for introduction of the discharge gas. The microwave frequency of 2450 MHz was produced by a Burdick model MW-200 microwave diathermy unit and fed to the cavity via coaxial wave guide. The cavity-wave guide vacuum seal was made by O-rings seated in teflon plug which

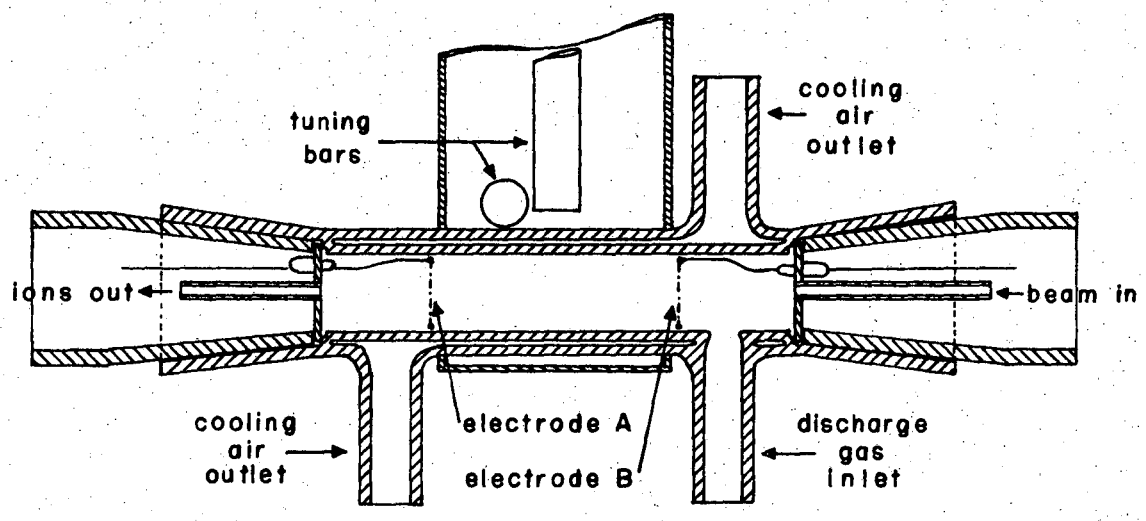

XBL 6711-6034

Fig. 13. Cutaway view of the microwave cavity and discharge tube.

also served as a support for the center conductor of the wave guide. The whole assembly was mounted on one of the main chamber port covers. Provision was made so that the cavity and discharge tube could be moved while under vacuum so that beam alignment could be performed. The tuning stubs were also adjustable from outside.

Initially the beam entrance consisted of a 10 mil slit in a flat disk placed on the end of the discharge tube and the ion exit consisted of a 1/32 in. diam hole in a similar disk. It was immediately obvious that the entrance and exit apertures were unsatisfactory since the pumping speed of the chamber was inadequate to maintain 10^{-6} mm Hg while the discharge tube maintained about 30-50 μm Hg which was necessary to obtain a stable discharge. The final working design of the apertures are shown in Fig. 13 along with the ion extraction electrodes which were made of tungsten wire mesh. The necessity of designing the apertures in channel form certainly is a serious problem both in alignment and ion extraction. However, if the carrier or discharge gas is He, Ne or Ar, elements which require less energy to ionize will be maintained in ionic form even while traveling through the long metal tube at ground potential due to a buffering effect of the carrier gas.

A quadrupole residual gas analyzer (Electronic Associates, Inc., Palo Alto, California) or mass filter was used to obtain mass spectra from the ion output of the discharge. Typical mass spectra of the ions extracted from He, Ne, and Ar discharges are shown in Figs. 14, 15 and 16. The background intensities, which are especially high for the Ne and Ar discharges are primarily due to Auger de-excitation of excited species on the first dynode of the electron multiplier. Since they are non-ionized species they are not affected by the mass filtering electric fields of the quadrupole. This effect can thus be largely eliminated by placing the quadrupole axis at a slight angle to the ion beam axis. Since the Ne discharge seemed to give the best operating conditions with respect to discharge stability and main chamber pressure (see Table A-V), it was used while attempting to detect a molecular beam. Several gases, namely HCl, SO_2 and H_2S were used as beam material as well as the condensible LiF. Unfortunately these experiments were unsuccessful. The only indi-

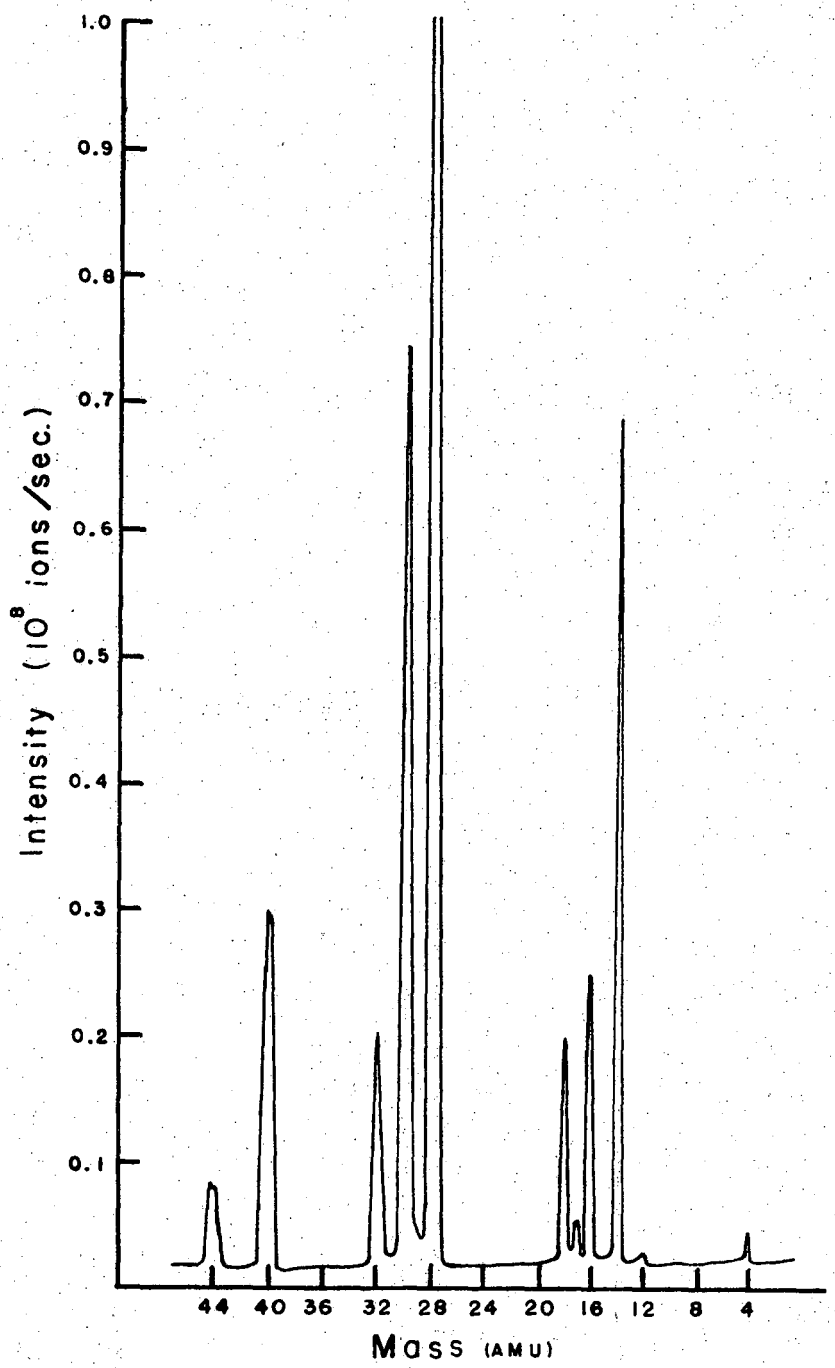

XBL 6711-6040

Fig. 14. Mass spectrum produced by a He discharge at 0.14 mm Hg pressure.

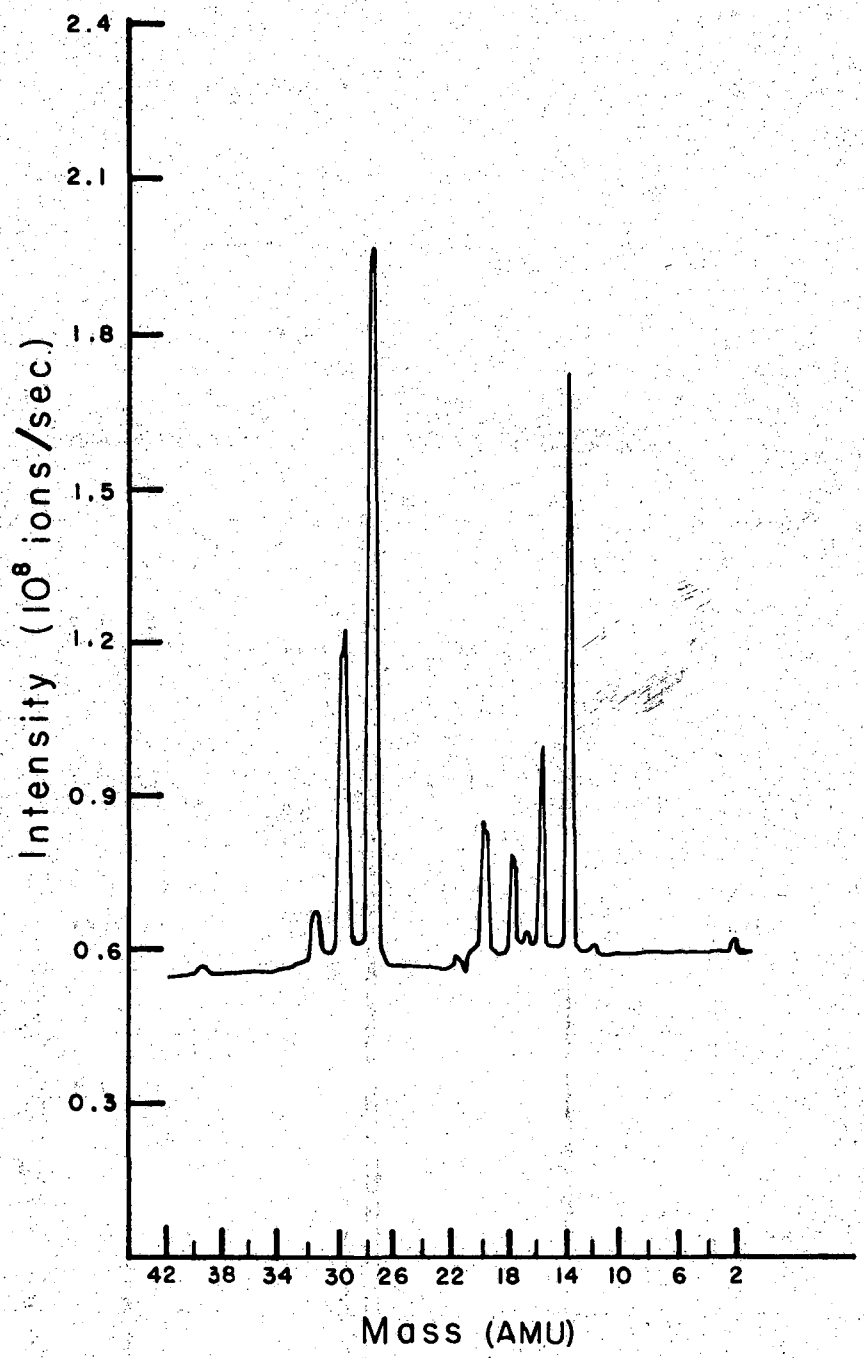

XBL 6711-6031

Fig. 15. Mass spectrum produced by a Ne discharge at 0.1 mm Hg pressure.

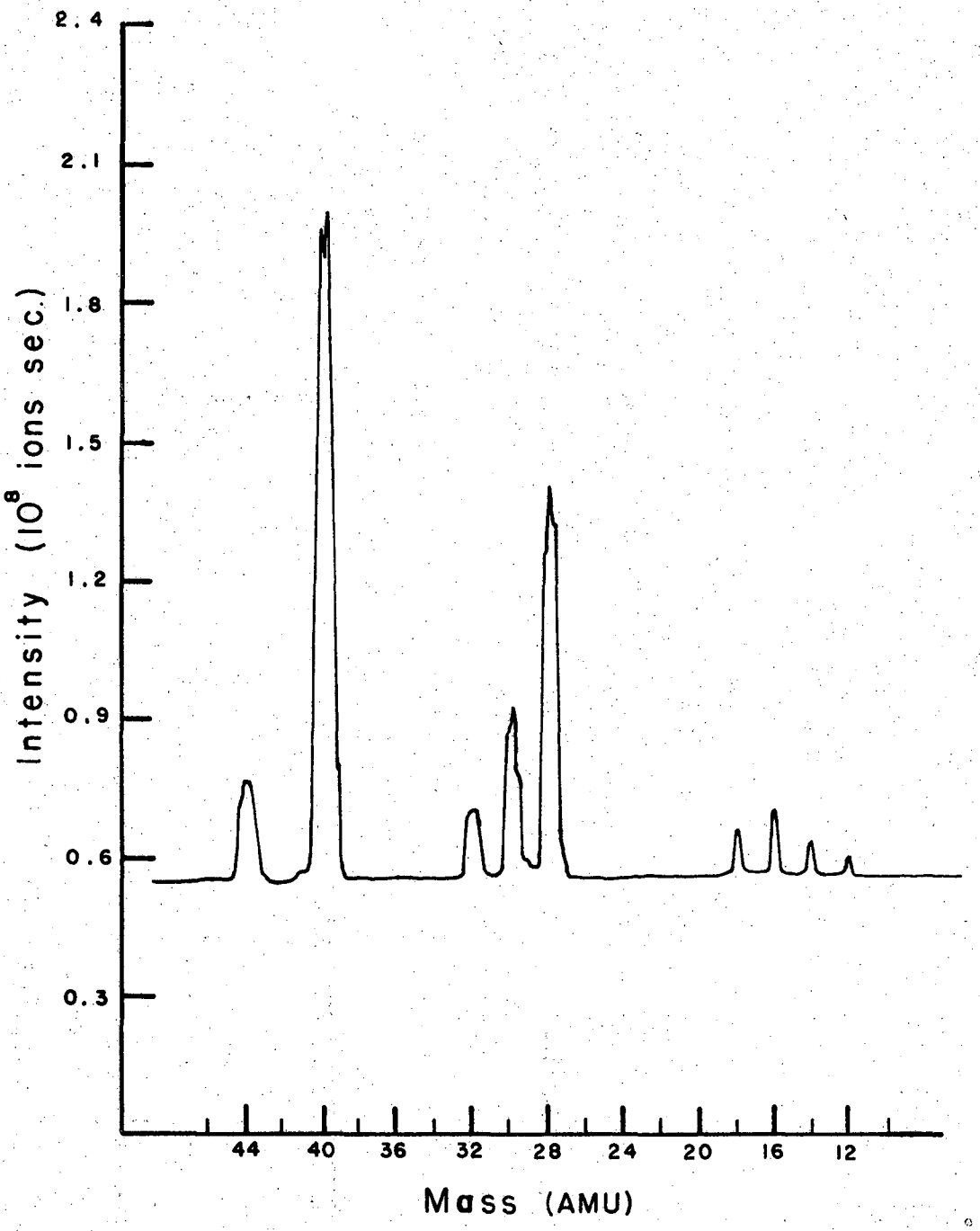

XBL 6711-6030

Fig. 16. Mass spectrum produced by an Ar discharge at 0.07 mm Hg pressure.

Table A-V. Operating characteristics of microwave cavity and discharge in high vacuum.

Discharge Gas	Chamber Pressure (mm Hg)	Discharge Tube Pressure (mm Hg)	Forward Wave Power (120 watts max)	Discharge
Ar	2.2×10^{-6}	0.035	10%	Stable
		0.020	10%	Stable
		0.015	10%	Extinguishes
		0.015	25%	Unstable
Ne	1.8×10^{-6}	0.100	10%	Stable
	1.5×10^{-6}	0.050	10%	Unstable
He	2.5×10^{-6}	0.100	10%	Unstable
		0.100	20%	Stable

cation of detection of the beam material was with HCl where a weak mass peak at mass 35 appeared but would not disappear when the beam was attenuated. This seems to indicate a long time constant, however, a rough calculation which assumes ideal gas behavior, a discharge tube volume of 5.3 cc and gas temperature of 1300°C indicates that a complete change in volume occurs every millisecond which suggests a short time constant in response.

The most likely reason that a beam was not detected is that beam scatter was too great since the discharge gas was also acting as a beam source. This likelyhood is reinforced by the fact that a long channel entrance was necessary. The mean free path in the channel is quite short which would mean several collisions would occur before a molecule could enter the discharge region.

Although this technique does not seem to be useful for beam detection, the device constructed does serve as and ion and excited state source as the spectra shown above indicate. The species shown in the three figures are most likely due to the fact that the quartz tube was cleaned with alcohol previous to use and also to organic impurities in the inert gas cylinders supplying the discharge gas. If one would like to produce an ion beam of a condensible substance, it would seem to suffice to coat the inside of the discharge tube with the substance or make the extracting electrodes of it. This type of ion source also has the potential to produce multiply charged species in somewhat greater quantities than possible by other methods.

Table B-I. Multichannel analyzer data retrival system electronic equipment.

Unit	Model	Manufacturer
Transistorized linear pulse amplifier		LRL[a] Plan No. 15X4845
Inverting amplifier (gain 1-10X, zero offset)		LRL[a] Plan No. 13X1450
Frequency or pulse scaler (0 to 10^8 counts/sec; with 5253A and 5253B plug-ins the counting range is extended to 500 MHz).	5245L	Hewlett-Packard Co. Palo Alto, Calif.
Radio frequency signal generators:		
a) 50 kHz to 65 MHz.	606B	Hewlett-Packard Co.
b) 10 MHz to 455 MHz.	608F	Palo Alto, Calif.
Digital recorder with analog output	562A	Hewlett-Packard Co.
Frequency synchronizer (locks 606B and 608F signal generators and allows modulation)	8708A	Hewlett-Packard Co. Palo Alto, Calif.
Frequency mixer (50 kHz to 450 MHz).	10514A	Hewlett-Packard Co.
Stark field voltage supply (1-6000 V at 20 mA)	HV-1556	Power Designs Pacific, Inc. Palo Alto, Calif.
Reference voltage supply (0-10 V)		LRL[a] Plan No. 13X1470
Ramp voltage generator		LRL[a] Plan No. 13X1430
Start pulse function generator		Electronics, Inc., Portland, Or.
Single channel analyzer	NC-11	Hammer Electronics Co., Inc. Princeton, New Jersey
Multichannel analyzer (1024 channels in quadrants, 2×10^5 sec dead time per channel)	NS-610	Northern Scientific Madison, Wisconsin
Data processor	460	Northern Scientific
Switch programed time base oscillator		LRL[a] Plan No. 15X8410
Programed coincidence scaler (0-9999 channels)		LRL[a] Plan No. 13X1310

[a]Lawrence Radiation Laboratory, Berkeley, California.

Table C-I. Dipole moment summary table.

Molecule	Vibrational state, v				Dipole moment function		
					$u_v = u_e + u_I(v+1/2) + u_{II}(v+1/2)^2$		
	v = 0	v = 1	v = 2	v = 3	u_e	u_1	u_{II}
$^{85}Rb^{19}F$[a]	8.5465(5)	8.6134(7)	8.6809(9)		8.5131(7)	0.06650(28)	0.00026(12)
[b]	8.5465(7)	8.6127(17)					
[c]	8.80(10)						
$^{85}Rb^{35}Cl$[a]	10.510(5)	10.564(5)	10.618(5)		10.483(6)	0.054(3)	
$^{133}Cs^{19}F$[a]	7.8839(9)	7.9546(10)	8.0257(10)	8.0969(15)	7.8486(13)	0.0704(3)	0.00018(20)
[d]	7.875(6)	7.9472(63)*	8.0194(66)*		7.839(6)*	0.0722(3)	
[e]	7.878(3)	7.950(3)			7.842(3)*	0.07229(12)	
[f]	7.3(5)						
$^{133}Cs^{35}Cl$[a]	10.387(4)	10.445(4)	10.503(4)		10.358(5)	0.058(1)	
[g]	10.42(2)	10.476(22)*	10.532(24)*		10.392(20)*	0.056(2)	
$^{23}Na^{127}I$[a]	9.2357(30)	9.2865(30)	9.3368(30)		9.2103(30)	0.0507(8)	

*Calculated here from reference indicated. All values are given in Debyes.

[a]Present work [c]Ref. 22 [e]Ref. 26 [g]Ref. 28 and 4

[b]Ref. 24 [d]Ref. 3 and 4 [f]Ref. 1

REFERENCES

1. H. K. Hughes, Phys. Rev. 72, 614 (1947).
2. J. W. Trischka, Phys. Rev. 74, 718 (1948).
3. J. W. Trischka, Phys. Rev. 76 (9), 1365 (1949).
4. John Trischka, J. Chem. Phys. 25, 784 (1956).
5. P. Kusch and V. W. Hughes, "Atomic and Molecular Beam Spectroscopy", in Handbuch der Physik, ed. by S. Flugge, 37/1 (Springer-Verlag, Berlin, 1959).
6. P. A. Bonczyk, Bulletin of American Physical Society 11 (1), 132 (1967).
7. R. van Wachem and A. Dymanis, J. Chem. Phys. 46 (10), 3749 (1967).
8. G. Gräff and G. Werth, Z. Physik 183, 223 (1965).
9. F. W. Breivogel, Jr., A. J. Hebert, and K. Street, Jr., J. Chem. Phys. 42 (5), 1555 (1967).
10. Robert S. Freund and William Klemperer, J. Chem. Phys. 43 (7), 2422 (1965).
11. Jens C. Zorn, Thomas C. English, J. Thomas Dickenson and David A. Stephenson, J. Chem. Phys. 45 (10), 3731 (1966).
12. R. Weiss, Phys. Rev. 131, 659 (1963).
13. A. J. Hebert, A Molecular-Beam Electric-Resonance Spectrometer and the Radio-Frequency Spectra of Lithium Fluoride (Ph.D. Thesis), UCRL-10482, September 1962.
14. N. F. Ramsey, Molecular Beams (Clarendon Press, Oxford, 1956).
15. N. F. Ramsey, Phys. Rev. 91, 303 (1953).
16. W. Drechsler and G. Gräff, Z. Physik 163, 165 (1961).
17. F. W. Breivogel, The Radio-Frequency and Microwave Spectra of LiBr and LiI (Ph.D. Thesis), UCRL-11665, September 1964.
18. C. D. Hollowell, The Molecular-Beam Electric-Resonance Spectra of LiF, NaF, and KCl (Ph.D. Thesis), UCRL-17019, November 1966.
19. V. W. Hughes and L. Grabner, Phys. Rev. 79, 819 (1950).
20. P. A. Bonczyk, The Hyperfine Structure of ^{85}RbF and ^{87}RbF by the Molecular-Beam Electric-Resonance Method (Ph.D. Thesis), Yale University, 1965; and V. W. Hughes, Phys. Rev. 161 (1), 15 (1967).

21. J. W. Trischka and R. Braunstein, Phys. Rev. 96, 968 (1954).

22. H. Lew, P. Morris, F. Geiger, Jr. and J. T. Eisinger, Can. J. Phys. 36, 171 (1958).

23. S. E. Veazey and Walter Gordy, Phys. Rev. 138 (5A), 1303 (1965).

24. G. Gräff, R. Schönwasser and M. Tonutti, Zeit. f. Phys. 199, 157 (1967).

25. Thomas C. English, A High-Resolution Measurement of the Hyperfine Structure of the J = 1 Rotational State of $^{133}Cs^{19}F$ by the Molecular Beam Electric-Resonance Method (Ph.D. Thesis), University of Michigan, 1966.

26. G. Gräff and Ö. Runolfsson, Zeit. f. Phys. 187, 140 (1965).

27. Jon H. Shirley, J. Chem. Phys. 38 (12), 2896 (1963).

28. R. G. Luce and J. W. Trischka, J. Chem. Phys. 21 (1), 105 (1953).

29. A. Honig, M. Mandel, M. L. Stitch and C. H. Townes, Phys. Rev. 96 (3), 629 (1954).

30. R. E. Cote and P. Kusch, Phys. Rev. 90, 103 (1953).

31. N. F. Ramsey, Molecular Beams (Clarendon Press, Oxford, 1956) p. 16.

32. Gerhard Herzberg, Spectra of Diatomic Molecules (D. Van Nostrand Co., In., Princeton, New Jersey) pp. 121-125, 1959.

33. G. Gräff and Ö. Runolfsson, Zeit. f. Phys. 176, 90 (1963).

34. Carl E. Miller and Jens C. Zorn (Randall Laboratory of Physics, University of Michigan, Ann Arbor) private communication, July 1967.

35. M. Born and W. Heisenberg, Z. Physik 23, 388 (1924).

36. M. Born and J. E. Mayer, Z. Physik 75, 1 (1932).

37. P. Debye, Polar Molecules (Dover Publications, New York, 1945).

38. E. S. Rittner, J. Chem. Phys. 19, 1030 (1951).

39. L. Pauling, Proc. Roy. Soc. (London) A114, 191 (1927).

40. Carlos A. Melendres (University of California, Berkeley) private communication, October 1967.

41. J. L. Dunham, Phys. Rev. 41, 721 (1932).

42. W. Klemperer and S. A. Rice, J. Chem. Phys. 26, 618 (1957).

43. S. A. Rice and W. Klemperer, J. Chem. Phys. 27, 573 (1957).

44. W. Klemperer, W. G. Norris and A. Buchler, J. Chem. Phys. 33, 1534 (1960).

45. A. J. Hebert, C. D. Hollowell, T. L. Story, and K. Street, Jr., University of California Lawrence Radiation Laboratory Report, UCRL-10482, March 1967.

46. Linus Pauling, The Nature of the Chemical Bond (Cornell University Press, Ithaca, New York, 1960) p. 526.

47. G. Burns, Phys. Rev. 115, 357 (1959).

48. R. M. Sternheimer, Phys. Rev. 115, 1198 (1959).

49. K. Street, Jr. (University of California, Berkeley) private communication, July 1967.

50. F. London, Z. Physik 63, 245 (1930).

51. C. E. Moore, U. S. Nat. Bur. of Standards Circ. No. 467 Vol. 1 (1949), Vol. 2 (1952), and Vol. 3 (1958).

52. R. S. Berry and C. W. Reimann, J. Chem. Phys. 38, 1540 (1963).

53. Leo Brewer, The Thermodynamic Properties of the Alkali Halides, UCRL-9952, November 1961.

54. L. Wharton, W. Klemperer, L. P. Gold, R. Strauch, J. J. Gallagher and V. E. Derr, J. Chem. Phys. 38, 1203 (1963).

55. G. L. Vidale, J. Phys. Chem. 64, 314 (1960).

56. D. R. Lide, Jr., P. Cahill and L. P. Gold, J. Chem. Phys. 40, 156 (1964).

57. J. R. Rusk and W. Gordy, Phys. Rev. 127, 817 (1962).

58. A. J. Hebert, F. W. Breivogel, Jr. and K. Street, Jr., J. Chem. Phys. 41, 2368 (1964).

59. W. Klemperer, W. G. Norris, A. Buchler and A. G. Emslie, J. Chem. Phys. 33, 1534 (1961).

60. R. K. Bauer and H. Lew, Can. J. Phys. 41, 1461 (1963); 42, 830 (1964).

61. C. D. Hollowell, A. J. Hebert and K. Street, Jr., J. Chem. Phys. 41, 3540 (1964).

62. R. K. Ritchie and H. Lew, Can. J. Phys. 42, 43 (1964).

63. P. L. Clauser and W. Gordy, Phys. Rev. 134, A863 (1964).

64. B. P. Fabricand, R. O. Carlson, C. A. Lew and I. I. Rabi, Phys. Rev. 91, 1403 (1953).

65. L. Wharton, M. Kaufman, and W. Klemperer, J. Chem. Phys. 37, 621 (1962).

66. M. Kaufman, L. Wharton, and W. Klemperer, J. Chem. Phys. 43, 943 (1965).

67. John Olmsted III, Amos S. Newton, and K. Street, Jr., J. Chem. Phys. 42 (7), 2321 (1965).

68. K. H. Kingdon and I. Langmuir, Phys. Rev. 21, 380 (1923).

69. H. E. Ives, Phys. Rev. 21, 385 (1923).

70. E. Ya. Zandberg and N. I. Ionov, Usp. Fiz. Nauk. 57, 581 (1959) or Soviet Physics Uspehki 67 (2), 255 (1959) in English.

71. Joseph R. Werning, Thermal Ionization at Hot Metal Surfaces (Ph.D. Thesis), University of California, Berkeley, UCRL-8455, September 1958.

72. The author is indebted to Fred Reynolds for providing several 1 × 20 mil (110) surface tungsten filaments for this work.

73. W. Weiershausen, "Investigation of the Adsorption of Oxygen on Tungsten by Mass Spectrometry", in Advances in Mass Spectrometry (MacMillen Co., New York, 1963, 1963), Vol. 2.

74. P. O. Schessel and O. C. Trulson, J. Chem. Phys. 43 (2), 737 (1065).

75. Fred Reynolds (University of California Lawrence Radiation Laboratory, Berkeley), private communication, August 1967.

76. F. C. Fehsenfeld, K. M. Evenson, and H. P. Broida, Rev. Sci Instr. 36 (3), 294 (1965).

77. Handbook of Chemistry and Physics, (The Chemical Rubber Co., Cleveland, 1967), 48th edition.

78. Erwin W. Muller, J. Appl. Phys. 26 (6), 732 (1955).

79. F. L. Reynolds, J. Chem. Phys. 39 (4), 1107 (1963).

80. George F. Smith, Phys. Rev. 94 (2), 295 (1954).

81. Sheldon Ira Schreiner, Thermionic Emission from Planar Monocrystaline Tungsten (M.S. Thesis), UCRL-16699, 1966.

82. E. P. Sytoya, M. I. Smorodinova, and N. I. Imargolova, Soviet Phys. - Solid State (English transl.) 4 (4), 750 (1962).

83. Daniel René Koenig, Surface Ionization of Cesium and Thermionic Emission from Planar Single Crystals of Tungsten (Ph.D. Thesis), UCRL-11857, 1966.

84. C. A. Haque and E. E. Donaldson, Rev. Sci. Instr. 34 (4), 409 (1963).

85. R. van Wachem, F. H. deLeeuw, and A. Dymanus, J. Chem. Phys. 47 (7), 2256 (1967).

This report was prepared as an account of Government sponsored work. Neither the United States, nor the Commission, nor any person acting on behalf of the Commission:

A. Makes any warranty or representation, expressed or implied, with respect to the accuracy, completeness, or usefulness of the information contained in this report, or that the use of any information, apparatus, method, or process disclosed in this report may not infringe privately owned rights; or

B. Assumes any liabilities with respect to the use of, or for damages resulting from the use of any information, apparatus, method, or process disclosed in this report.

As used in the above, "person acting on behalf of the Commission" includes any employee or contractor of the Commission, or employee of such contractor, to the extent that such employee or contractor of the Commission, or employee of such contractor prepares, disseminates, or provides access to, any information pursuant to his employment or contract with the Commission, or his employment with such contractor.